Prabha Materials Science Letters
Vol. 5, No. 1, 74-102, 2026
https://doi.org/10.33889/PMSL.2026.5.1.005

A Comprehensive Review on the Synthesis, Characterization, and Applications of Spinel Ferrite Nanoparticles

P. Swetha
PG & Research Department of Physics,
St. Joseph's College of Arts and Science (Autonomous),
Annamalai University, 607001, Cuddalore, Tamil Nadu, India.
E-mail: swetha24162@gmail.com

R. Sagayaraj
PG & Research Department of Physics,
St. Joseph's College of Arts and Science (Autonomous),
Annamalai University, 607001, Cuddalore, Tamil Nadu, India.
Corresponding author: sagayarajnancy@gmail.com

(Received on October 11, 2025; Revised on January 14, 2026; Accepted on January 26, 2026)

Abstract
Spinel ferrite materials, particularly spinel ferrites, have gained immense popularity due to their unique magnetic properties and versatility in modern technology. With the general formula AB_2O_4, where A and B are metal cations, these materials can be classified as soft or hard ferrites, each with distinct applications ranging from microwave components and inductors to permanent magnets and data storage. This review focuses on the synthesis and characterization of spinel ferrite nanoparticles. We examine various synthesis methods, including co-precipitation, sol-gel, hydrothermal, and combustion techniques, highlighting their respective advantages and disadvantages in terms of cost, particle size control, and purity. The review also details the use of advanced characterization techniques. X-ray Diffraction (XRD) is crucial for confirming crystal structure, phase purity, and determining crystallite size and lattice constants, while Fourier-Transform Infrared (FTIR) spectroscopy identifies characteristic metal-oxygen bonds. Furthermore, Electron Microscopy (TEM and SEM) is used to analyse particle morphology, size, and agglomeration, and Vibrating Sample Magnetometry (VSM) is essential for evaluating key magnetic properties like saturation magnetization and coercivity. The review synthesizes findings from a wide range of studies, underscoring the critical relationship between synthesis parameters, doping, and the resulting structural and magnetic properties of these nanomaterials, which are key to their functional applications in fields like targeted drug delivery and magnetic resonance imaging.

Keywords- Spinel ferrite, Nanoparticles, Magnetic properties, VSM, XRD, Magnetic resonance imaging.

1. Introduction

Ferrites, which have iron as their primary constituent, are magnetic materials exhibiting ferromagnetic ordering. Iron oxide, which is found in nature, comes in pure forms such magnetite (Fe_3O_4), hematite (Fe_2O_3), iron oxide beta phase, maghemite, and others. These substances exhibit unique colours, poor solubility, and trivalent oxidation states. Since magnetite (Fe_3O_4) contains both Fe^{2+} and Fe^{3+} ions, it is the most significant ferrite (Hemingway, 1990). Ferrites are becoming more and more popular because of their spontaneous magnetism (Torruella et al., 2018). The magnetic behavior of the ferrites is determined by the magnetic dipole moment related to the electron spin (Maji and Dosanjh, 2023). At temperatures below the Curie temperature (TC), ferrite materials display ferromagnetism, which turns into paramagnetic at temperatures over TC. With specific resistivities 10^{14} times higher than those of metals with dielectric constants of 10 to 16 or higher, ferrites exhibit extremely high electrical resistivity rather than conducting electricity as ferromagnetic materials do. As a result, they could be used as a magnetic core in transformers (Arcaro and Venturini, 2021). These ferrites are often categorized based on two distinct forms: Soft ferrites and Hard ferrites. Soft ferrites were found to have low coercivity, which allows magnetization to be

customized to the application's needs. As a result, the conducting nature of the magnetic field makes way for its numerous, significant applications in electronic engineering, including high-frequency inductors, microwave components, and emerging transformer cores (Herzer, 1990; Padmapriya et al., 2016). Hard ferrites have a high coercivity, which makes them difficult to magnetize (Xavier et al., 2013). As a result, they are used to make durable magnets, which are used in high-frequency applications, washing machines, refrigerators, communication systems, microwave absorbing systems, loudspeakers, TVs, switch-mode power supplies, and dc-dc converters (Mary et al., 2015). Spinel ferrites, with the general formula AB_2O_4, are a class of magnetic materials that have been extensively studied for their versatile applications in modern technology, where A is denoted by Fe, Co, Ni, Mg, Mn, Cu and Zn which are the divalent metal ions (Soufi et al., 2021). The microwave control components like circulators, phase shifters, and isolators are made by spinel ferrites (Hajalilou and Mazlan, 2016; Jayarajan et al., 2023). The unique crystal structure of spinel ferrites, consisting of a face-centred cubic (FCC) lattice of oxygen ions with tetrahedral (A) and octahedral (B) interstitial sites occupied by divalent and trivalent cations, gives rise to their remarkable magnetic and electrical properties (Naeem et al., 2009; Rafienia et al., 2018). More precisely, trivalent metals (Fe^{3+}) in the case of spinel ferrites occupy one-eighth of the octahedral B sites, whereas divalent cations (Fe^{2+}) occupy one-sixteenth of the tetrahedral locations (site A) (Arcaro and Venturini, 2021). The distribution of these cations between the A and B sites which can be normal, inverse, or mixed spinel ferrite which, plays a crucial role in determining the overall magnetic behavior of the material. Normal spinel ferrite is characterized by an orderly distribution of cation and anion sites inside the lattice, as in magnesium ferrite ($MgFe_2O_4$) (Veeramani et al., 2023), Zinc ferrite ($ZnFe_2O_4$) (Granone et al., 2018). It is referred to as inverse spinel ferrite when the cation and anion sites inside the lattice are arranged reversed, as in magnetite (Fe_3O_4) (Veeramani et al., 2023), $CuFe_2O_4$ (Gomes et al., 2005), $MgFe_2O_4$ (Khishigdemberel et al., 2018). This suggests that the magnetic characteristics of spinel ferrites may be influenced by the distribution of cations between the two interstitial sites (Xu et al., 2007). In the last three decades, the synthesis of ferrite nanoparticles has been playing avital role among young scientists for the reduction of particle size from bulk size to nano scale. Among which, superparamagnetism lead to novel signature properties such as magnetic properties, thermal stability, chemical stability, photocatalytic activity, high surface area and low cost (Tiwari et al., 2020). These properties are elucidated in the **Figure 1**.

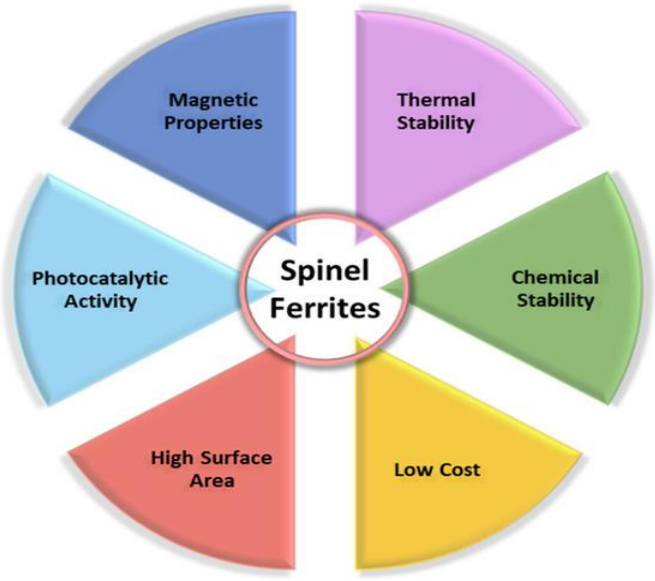

Figure 1. Figure illustrating spinel ferrite's properties (Maji and Dosanjh, 2023).

The ability to tune the magnetic properties of these nanoparticles by controlling their size, shape, and composition has opened up new possibilities for their use in advanced applications, including high-density data storage, targeted drug delivery, and magnetic resonance imaging (MRI) (Chandra et al., 2017).This review will focus on the synthesis and characterization of various spinel ferrite nanoparticles, with a particular emphasis on the effects of different dopants on their structural, morphological, and magnetic properties. We will also discuss the importance of various characterization techniques in understanding the behavior of these materials at the nanoscale and explore their functional applications.

2. Synthesis of Spinel Ferrite Nanoparticles

Spinel ferrite nanoparticles are synthesized using various methods, with its own advantages and disadvantages regarding the resulting particle size, shape, purity, and crystallinity. Prasad et al. (2021) explained that the synthesis methods can be broadly classified into "top-down" approaches like mechanical milling and "bottom-up" chemical techniques as shown in **Figure 2**. Rawat (2015) reported that the choice of method is critical as it directly influences the final properties of the material. While the "top-down" method depends on the sequential processing or fragmentation of macro-scale materials into smaller Nano-sized things, the "bottom-up" method builds nanoscale materials by assembling atoms and molecules.

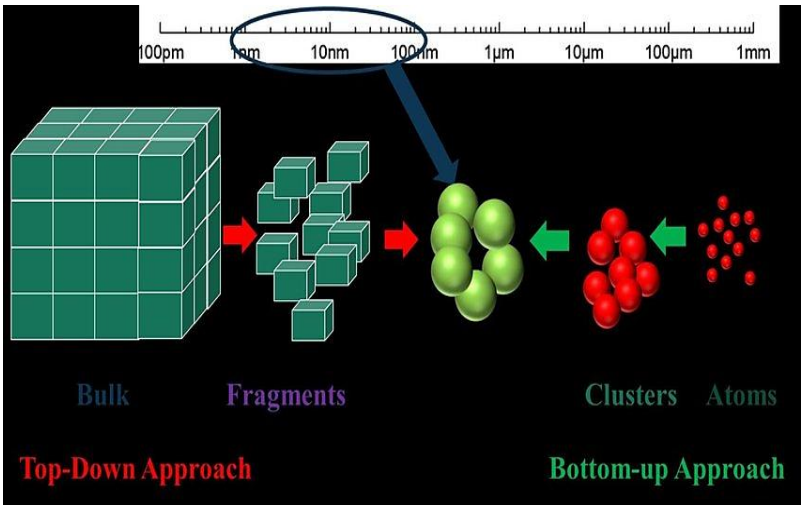

Figure 2. Schematic representation of top-down and bottom-up approach (Prasad et al., 2021).

Comparative Review of Fabrication Methods

Table 1 presents a comparative analysis of various fabrication techniques for synthesizing particulate materials, focusing on their cost-effectiveness, particle nature, and technical attributes, as well as their respective advantages and disadvantages, each supported by relevant references. The methods evaluated are commonly used in materials science to achieve desired morphological and crystalline properties in advanced applications.

2.1 Co-precipitation Method

The co-precipitation method stands out for its simplicity, rapid process, and ability to produce a high yield of particles at a low cost. However, this approach generally results in particles with poor uniformity and high agglomeration, often presenting a broad size distribution, which can hinder applications requiring precise control over nanostructure properties. According to Mayura and Jayasimhadri (2024), these

drawbacks restrict its use for critical functions requiring particle homogeneity. This is one of the most widely used wet chemical methods. It involves dissolving metal salts (e.g., nitrates, chlorides) in an aqueous solution and then adding a precipitating agent (like sodium hydroxide or ammonium hydroxide) to adjust the pH which was reported by Peng et al. (2021). The metal ions precipitate as hydroxides, which are then heated to form the spinel ferrite structure. This method is praised for its simplicity, high yield, and ability to produce nanoparticles with a narrow size distribution.

Co-precipitation method has been used to create a range of spinel ferrites, notably $MgFe_2O_4$ (Kaur and Kaur, 2014), $CuFe_2O_4$ (Wu et al., 2004), $CoFe_2O_4$ (Vinosha and Das, 2018; Selvam et al., 2024), $MnFe_2O_4$ (Khan et al., 2019) etc. Thakur et al. (2020) reported that the chemical co-precipitation approach involves mixing aqueous solutions of Mn^{2+}, Zn^{2+}, and Fe^{3+} nitrates to create a homogenous solution, which is then precipitated as mixed metal hydroxides by adding ammonia to maintain pH between 10 and 11. $Mn(OH)_2$, $Zn(OH)_2$, and $Fe(OH)_3$ precipitate simultaneously in the alkaline media, assuring a consistent distribution of cations. The nucleation and development of the hydroxide precursors are encouraged by heating and age. Through solid-state diffusion and dehydration, the mixed hydroxides are further calcined at high temperatures to form crystalline $Mn_{0.5}$ $Zn_{0.5}$ Fe_2O_4 spinel ferrite. It involves the simultaneous precipitation of divalent and trivalent metal ions from an aqueous solution using a base, such as ammonia, to maintain a high pH (typically ~11). The precipitate is then washed, dried, and calcined as shown in **Figure 3**. For instance, PVP-coated $ZnFe_2O_4$ nanoparticles synthesized this way show a normal spinel structure with a crystallite size of approximately 11.14 nm which was reported by Sagayaraj et al. (2017). This method has also been used to produce cobalt ferrites ($CoFe_2O_4$) with an average crystallite size of 9 nm (Sagayaraj et al., 2019b) and zinc-doped manganese ferrites ($Mn_{1-x}Zn_xFe_2O_4$) with sizes around 20.61 nm (Poongodi et al., 2024). The use of Polyvinylpyrrolidone (PVP) as a surfactant is common to control agglomeration (Sagayaraj et al., 2019a). A variation of the co-precipitation technique, this method uses oxalate precursors. It has been successfully employed to synthesize rare-earth doped ferrites like Terbium-Nickel ferrite ($Ni_{0.5}Tb_{0.5}Fe_2O_4$). The resulting nanoparticles were found to be polycrystalline with a crystallite size of 10 nm (Sagayaraj et al., 2020).

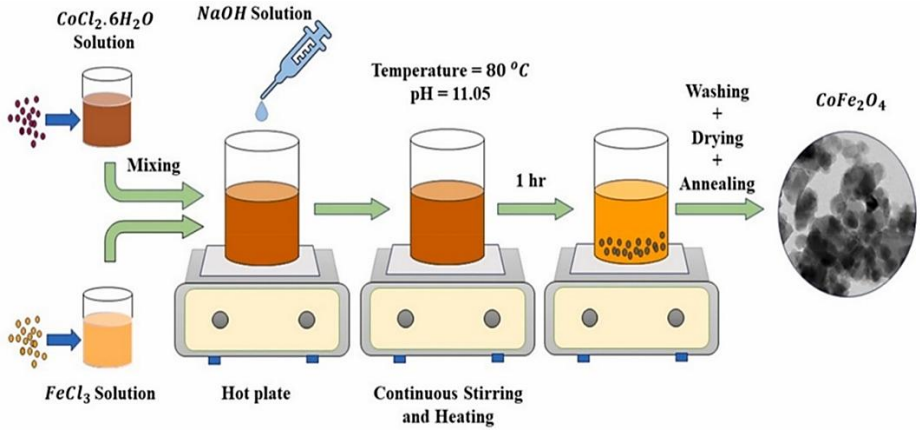

Figure 3. Schematic diagram of the sample preparation of $CoFe_2O_4$ by co-precipitation method (Roy et al., 2024).

When different solubilities like Fe^{3+} hydroxides which precipitate at a lower pH (around 2-3) and divalent ferrite cations which leads to precipitation at higher pH (8-11), this disrupts the consistency unless pH is carefully balanced. As a result, there occurs sequential precipitation rather than co-precipitation, which causes non-stoichiometric product yielding with phase impurities or separated particles (Dippong et al.,

2021). Co-precipitation in Ni-Cu-Zn ferrites is difficult if Cu^{2+} (moderately soluble) and Fe^{3+} differ significantly from Zn^{2+}. This leads to agglomeration and poor crystallinity without precise pH control (7–12) (Peng et al., 2021). Co –Fe ferrites exhibit comparable problems, such as extensive agglomeration and a wide range of particle sizes when the hydrolysis rates of salts such as sulphates or chlorides are not aligned. Although strict pH control or sequential addition can minimize these defects but cannot be completely removed (Dippong et al., 2021).

2.2 Sol-Gel Synthesis and Microwave-assisted Synthesis

Methods such as sol-gel and microwave-assisted synthesis are praised for producing homogeneous, high-purity materials, especially suitable for thin films and applications demanding a uniform particle morphology. The sol-gel process offers high purity and good control, but is hampered by procedural complexity and costly precursors, as noted in Reference (Nassar et al., 2025). On the other hand (Bao et al., 2023) reported, microwave-assisted synthesis enables extremely fast and energy-efficient fabrication with low agglomeration, though scalability.

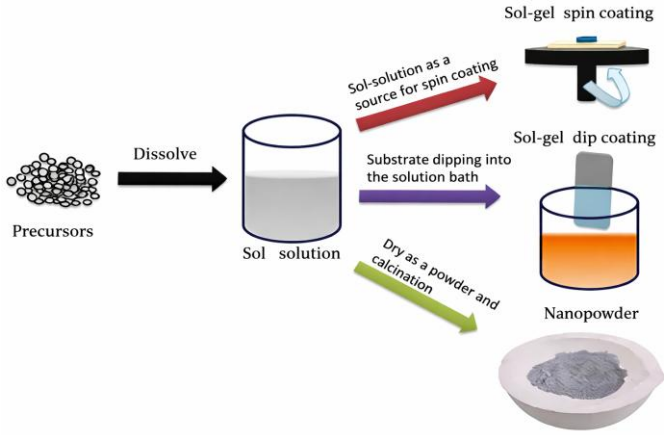

Figure 4. Schematic representation of Sol-Gel Synthesis of nanoparticles (Nassar et al., 2025).

This is a versatile and effective method for creating a wide range of materials. By using Sol-Gel approach, several spinel ferrites have been created, including $NiFe_2O_4$ (Ahlawat et al., 2011), $ZnFe_2O_4$ (Sutka et al., 2013), $CaFe_2O_4$ (Khanna and Verma, 2013) etc. It begins with a solution of metal precursors (the "sol"), which is then hydrolysed and condensed to form a gel. The gel is subsequently dried and subjected to calcination (heat treatment) to remove organic matter and form the final crystalline ferrite nanoparticles (Somvanshi et al., 2020) as shown in **Figure 4**. Veeramani et al. (2023) reported that the sol-gel method offers excellent control over the material's homogeneity and can produce very fine, highly pure nanoparticles. The sol-gel method involves the formation of a sol (a colloidal suspension) followed by its conversion into a gel with a three-dimensional network. The gel is then dried and calcined. This method has been used to synthesize $Mg_{1-x}Zn_xFe_2O_4$ nanocomposites, which exhibit a cubic spinel structure with crystallite sizes ranging from 19 to 40 nm. The sol-gel method generally offers better control over particle morphology and purity compared to co-precipitation, though it is a more complex process.

2.3 Hydrothermal Synthesis

The hydrothermal synthesis process delivers improved control over particle size and morphology and produces materials with high crystallinity. While these attributes make it suitable for specialized applications, the necessity for high pressure and temperature, coupled with specialized equipment, increases

both operational complexity and cost. Reference emphasizes its utility in fine-tuning particle characteristics for functional materials, though practical barriers which was reported by Phong et al. (2019). Thakur et al. (2020) said that this method involves carrying out chemical reactions in a sealed vessel called an autoclave at high temperatures and pressures as shown in **Figure 5**. When water is used as the solvent, it's called hydrothermal synthesis, and when organic solvents are used, it's called solvothermal synthesis. This technique is advantageous because it can produce highly crystalline nanoparticles without the need for a separate high-temperature annealing step, leading to better control over particle size and shape said by Rafienia et al. (2018).

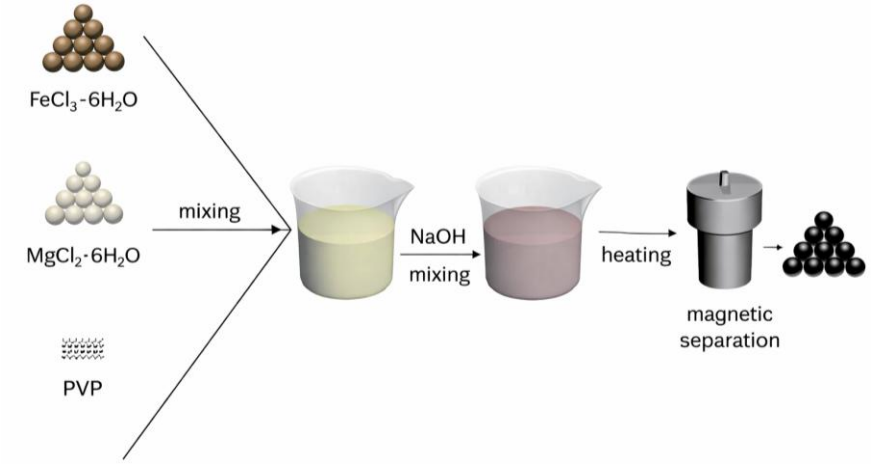

Figure 5. Hydrothermal synthesis of nanoparticles (Zheng et al., 2018).

When creating ferrite nanostructures with regulated morphologies, like nanorods or nanospheres, the hydrothermal approach is especially helpful (Phong et al., 2019). Using Hydrothermal/Solvothermal method many spinel ferrites have be synthesized, they are $CuFe_2O_4$ (Moreno- Castilla et al., 2019), $NiFe_2O_4$ (Liu et al., 2012), $ZnFe_2O_4$ (Su et al., 2012), $MgFe_2O_4$ (Zheng et al., 2018) etc.

2.4 Combustion Method

Auto-combustion and thermal decomposition techniques can yield crystalline powders directly and ensure excellent size uniformity and monodisperse distribution, especially in thermal decomposition methods. The latter, Salih et al. (2023) ensured that there exists outstanding control over particle size and shape but demands high temperatures and expensive organic solvents. Auto-combustion offers a simpler and faster route, albeit with difficulties in controlling impurities and reaction conditions, according to Singh et al., (2020). This is a quick and energy-efficient method. It involves mixing metal nitrates (oxidizers) with an organic fuel (such as urea or glycine). The mixture is ignited, leading to a rapid, self-sustaining exothermic reaction that quickly forms the spinel ferrite nanoparticles. This method is known for producing homogeneous, crystalline powders in a short amount of time and at relatively low temperatures. By using combustion method various spinel ferrites are created, notably $CoFe_2O_4$ (Prabhakaran and Hemalatha, 2016) and $NaFe_2O_4$ where, the combustion process involves direct atomic-scale mixing of the cations. The method's fuel, oxalyl dihydrazide ($C_2H_6N_4O_2$), facilitates the combustion synthesis of ferrites. The exothermic redox chemical reaction releases a vast amount of heat and gases (CO_2, N_2, H_2O vapor), which not only lowers the external temperature needed to prepare ferrites but also dissipates the heat, preventing the sintering of small ferrite particles confessed by Randhawa and Gandotra (2009).

2.5 Citrate Combustion Method

Finally, the citrate combustion method is noted for its simplicity and non-toxicity, making it accessible for many laboratories. However, this method is challenged by increased porosity, high agglomeration, and less control over particle size, limiting its application potential. As per Al Kiey et al. (2022) while effective for certain tasks, controlling particle characteristics remains a prominent limitation. From an academic viewpoint, method selection is critically linked to material requirements such as particle morphology, crystallinity, and agglomeration behavior. Techniques like hydrothermal and thermal decomposition are favoured for advanced research where uniformity and high crystallinity are essential, while simpler, cost-effective methods like co-precipitation and citrate combustion may suffice for bulk production or initial exploratory studies. Referenced studies emphasize trade-offs between process complexity, cost, and functional outcomes, guiding scholars toward tailored synthesis strategies per application needs. By combining iron and bismuth nitrates with citric acid as a fuel and complexing agent, the citrate combustion process creates $BiFeO_3$ nanoparticles. A self-propagating exothermic reaction is initiated by grinding precursors, heating them to a viscous gel, and igniting them. The fluffy ash from this quick combustion is calcined at about 600°C to create pure, single-phase rhombohedral nanoparticles (about 47 nm). It maintains atomic uniformity, keeps impurities and solvents out, and improves multiferroic qualities discussed by Layek and Verma (2015).

Table 1. Analysis of fabrication techniques, highlighting the relationship between method selection and resulting material characteristics, including cost-effectiveness and process limitations.

Method	Cost	Particle nature	Agglomeration	Morphology	Crystallinity	Advantages	Disadvantages	Reference
Co-precipitation	Low	Poor	High	Spherical	Moderate	Simple, fast, high yield.	Broad size distribution, high agglomeration.	Maurya and Jayasimhadri (2024)
Hydrothermal	Moderate	Good	Low	Faceted, Spherical	High	Good control over size and morphology, high crystallinity.	Requires high pressure and temperature, specialized equipment.	Salavati-Niasari et al. (2010)
Sol-gel	Moderate	Good	Low-Moderate	Spherical	High	Homogeneous, high purity, good for thin films.	Can be complex, uses expensive precursors.	Nassar et al. (2025)
Auto-combustion	Low	Good	Moderate	Spherical, porous	High	Fast, simple, produces crystalline powders directly.	Can be difficult to control, potential for impurities from fuel.	Salih and Mahmood (2023)
Thermal Decomposition	High	Excellent	Very Low	Monodisperse, Spherical	Very High	Excellent control over size and shape, very uniform.	Requires high temperatures, organic solvents, expensive precursors.	Singh et al. (2020)
Microwave-assisted	Moderate	Good	Low	Spherical	High	Extremely fast, uniform heating, energy efficient.	Can be difficult to scale up, requires specialized equipment.	Bao et al. (2023)
Citrate combustion method	Low	Good	High	spherical and irregular	Large	Simple, Effective, Non-toxic	High agglomeration, Particle size control, Increased porosity	Al Kiey et al. (2022)

3. Characterization of Spinel Ferrite Nanoparticles

3.1 X-ray Diffraction (XRD)

A recurring theme is the notable effect of temperature and chemical environment on the resulting crystallite size and crystalline phase from **Table 2**. A recurring theme is the notable effect of temperature and chemical environment on the resulting crystallite size and crystalline phase. For instance, the $MgFe_2O_4$ spinel compound, when calcined at 700°C, exhibits considerable variation in crystallite size ranging from approximately 22 nm to 50 nm, indicating that even with fixed conditions, synthesis reproducibility can be challenged. Such variability is often attributed to precursor chemistry and processing nuances, as discussed by Gupta et al. (2020) and Mushtaq et al. (2024). Additionally, Fe_3O_4 produced at lower heating temperatures (200–300°C) consistently yields ultrafine crystallite sizes (4–6 nm), which are preferred for magnetic nanoparticle applications due to superparamagnetic behavior. Reference by Lu et al. (2011) emphasizes the importance of controlled thermal treatments for tailoring particle size. The table also shows how chemical additives affect ferrite properties. Application of surfactants like CTAB and SDS or adjustments to alkaline pH (e.g., pH-12) during the synthesis of $CoFe_2O_4$ results in smaller crystallite sizes (as low as 10–11 nm), alongside well-defined cubic spinel structures. These findings by Lu et al. (2011), Gupta et al. (2020) and Vishwas et al. (2022) suggest that surface-active agents and pH stabilization promote nucleation while hindering excessive growth and agglomeration, which is compatible with literature on surfactant-mediated nanomaterial synthesis.

Moreover, compounds such as $CoFe_{2-x}Gd_xO_4$ and $Co_{1-x}Ni_xFe_2O_4$ demonstrate that elemental substitution or doping (e.g., with Gd or Ni) as shown in **Figure 6** can slightly decrease both crystallite size and lattice constants, thus modifying the unit cell structure and potentially magnetic properties. These effects are highlighted by Melo et al. (2018), Yadav et al. (2018b) and Mushtaq et al. (2024) showing that chemical tailoring of spinel ferrites is a viable approach for bespoke functional materials. XRD is fundamental for confirming the crystal structure and phase purity. For PVP-coated $ZnFe_2O_4$, XRD analysis confirmed a normal spinel structure with a crystallite size of 11.14 nm. The octahedral and tetrahedral structure is affected when Zn is doped with Fe_2O_4 (Sagayaraj et al., 2017). Doping significantly affects structural parameters. For example, in Ce-doped $ZnFe_2O_4$, the crystallite size was observed to change from 12.6 nm to 44.2 nm and the lattice constant from 8.43 Å to 8.51 Å as the cerium concentration increased (Prakash et al., 2022). As all the lattice constant value is same, the nanoparticles are observed to have cubic structure (Sagayaraj et al., 2017). In contrast, doping $MgFe_2O_4$ with ZnO decreased the crystallite size from 40 nm to 19 nm (Veeramani et al., 2023). Because Zn^{2+} has a larger charge density than other metal ions and may dissolve more readily, its increased solubility in the matrix led to a drop-in crystallite size.

Further, the rate of nucleation and development was accelerated by the greater electrostatic interactions between Zn^{2+} and the structure of ions, which further reduced the size of the crystallites. Shorter bond lengths and a drop in the lattice constant are the results of the greater repulsive interactions between metal ions caused by higher charge density and smaller atomic radius of Zn^{2+} which was discussed by Veeramani et al. (2023). When Co^{2+} is doped with $Fe^{2+}Al_2^{3+}O_4^{2-}$ the crystallite size remains constant. The same crystallite size may have been produced by a combination of the synthesis process, reaction temperature, duration, precipitate quantity, and other variables (Poongodi et al., 2023). In Fe-Co-Al_2O_4 (600, 700, 800, 900, 1000ºC) spinel aluminates as the temperature increases the crystal lattice enlarges. Rising temperatures have the ability to eliminate contaminants and facilitate the creation of a homogeneous substance with the necessary characteristics. Higher temperatures enable more efficient ion diffusion, resulting in more ordered and distinct crystal structures, as indicated by an increase in lattice constant and crystallite size with higher annealing temperature. But when the sintering temperature rises, this effect reverses, increasing the lattice constant and crystallite size up to 900^0C (and further the size reduces at 1000ºC because the high temperature promotes more efficient atom and ion transport, a more ordered crystal structure with smaller

crystallite sizes (9.49 nm) is produced (Poongodi et al., 2023).

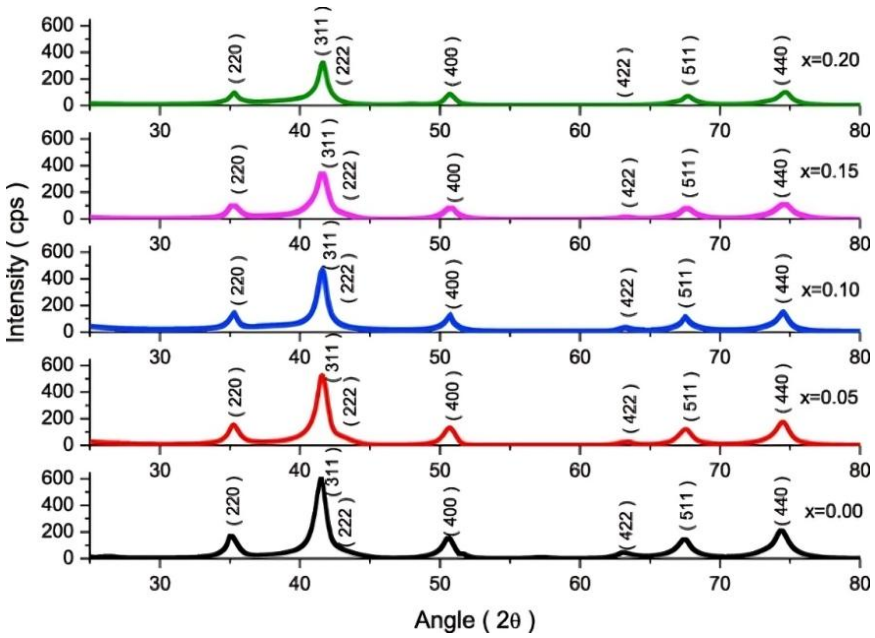

Figure 6. X-Ray diffraction patterns of $CoFe_2$-xGd_xO_4 nanoparticles (Yadav et al., 2018b).

Table 2. Synthesis pH, temperature, crystallite size, lattice constant, and crystal structure of the ferrite compound as a function of the surfactant used.

Ferrite Compound	Surfactant/pH	Condition	Crystallite size	Lattice constant	structure	Reference
$NiFe_2O_4$	cetyltrimethylammonium bromide (CTAB), sodium dodecylbenzene sulphonate (SDS) /pH- 11	Dried at 65°C	22nm and 27nm	996-	cubic inverse spinel	Mushtaq et al. (2024)
$SrFe_{12}O_{19}$	polyethylene glycol 6000 (PEG), CTAB, SDS	Calcined at 600 to 1000°C	40 – 30 nm	-	cubic spinel	Lu et al. (2011)
$CoFe_2O_4$	CTAB, SDS/pH-10	Calcined at 550°C	10.5 – 13.6 nm	8.309 – 8.336 A0	inverse spinel	Gupta et al. (2020)
$CoFe_2O_4$, $CuFe_2O_4$, Co–Cu Fe_2O_4	pH-7	Calcined 800°C	20, 24 and 22 nm	8.4, 5.9 and 8.42 A0	cubic spinel	Al kiey et al. (2022)
$CuFe_2O_4$, $ZnFe_2O_4$	-	150°C heating	31.42 and 30.74 nm	-	Spinel	Kanagesan et al. (2016)
$CoFe_2O_4$	pH-12	Annealed at 500°C	10.63 and 14.76 nm	8.3919 Ao	spinel	Vishwas et al. (2022)
$Co_xFe_{1-x}Fe_2O_4$	Tween 20, CTAB, SDS	Dried at 80°C	18.7 – 9.81 nm	8.32 to 8.35 Å	inverse spinel	Sangsuriyonk et al. (2022)
$CoFe_2O_4$, $NiFe_2O_4$, $ZnFe_2O_4$	Oil, pH-12	500 °C heating	11,4 and 14 nm	8.3961,8.3393 and 8.437 Ao	Cubic spinel	Rodriguez et al. (2019)
$Co_{1-x}Ni_xFe_2O_4$	pH-12	180°C	-	8.379 (2) and 8.346 (2) Å	cubic inverse spinel	Melo et al. (2018)
$CoFe_{2-x}Gd_xO_4$	-	Dried at 60 °C	9.2 nm to 7.6 nm	8.3752 Å to 8.3470 Å	Cubic spinel	Yadav et al. (2018b)
$FeTiO_3$		Dried at 200°C	31 nm		Mixed spinel	Shukla et al. (2018)

Across the compounds listed such as $MgFe_2O_4$, Fe_3O_4, $CoFe_2O_4$, $CuFe_2O_4$, $ZnFe_2O_4$, $NiFe_2O_4$, and $FeTiO_3$ which there is a strong correlation between synthetic methodology (calcination/annealing temperature, presence of surfactant, pH) and definitive structural parameters such as lattice constant and crystallite dimension, each critically affecting magnetic and electrical performance. These findings offer substantive insights for researchers aiming to engineer ferrite nanoparticles with tailored features by manipulating synthesis parameters. The referenced studies collectively advance the understanding of process-property relationships in ferrite chemistry, emphasizing that careful control over thermal, chemical, and compositional factors can yield materials with optimized nanostructure and, consequently, desirable functional characteristics in a given application.

3.2 Fourier-Transform Infrared Spectroscopy (FTIR)

FTIR spectroscopy is a crucial technique for identifying the characteristic metal-oxygen (M-O) bonds within the spinel lattice structure of ferrites, revealing two prominent absorption bands from **Table 3**. The higher frequency band (v_1) corresponds to the M-O stretching vibrations in the tetrahedral (A) sites, while the lower frequency band (v_2) is attributed to M-O vibrations in the octahedral (B) sites. The specific positions of these bands are sensitive to the material's composition. For example, in pure zinc ferrite ($ZnFe_2O_4$), these bands are observed near 540-550 cm^{-1} (v_1) and 455-470 cm^{-1} (v_2) (Sagayaraj et al., 2017), and similar ranges are seen for Cerium-doped $ZnFe_2O_4$ at 540-549 cm^{-1} (v_1) and 452-496 cm^{-1} (v_2) (Prakash et al., 2022). In comparison, cobalt ferrite ($CoFe_2O_4$) exhibits bands at 573 cm^{-1} (v_1) and 455 cm^{-1} (v_2) (Sagayaraj et al., 2019b), and Terbium-Nickel ferrite shows them at 584-610 cm^{-1} (v_1) and 412-422 cm^{-1} (v_2) (Sagayaraj et al., 2020), illustrating how cation substitution influences the vibrational energies within the spinel structure. The Sr-$CoFe_2O_4$ nanoparticles shows that, as the synthesis temperature rises from 75°C to 85°C, the transmittance of the FTIR spectrum increases observed by Prasetya et al. (2025). But at 95°C the transmittance seems to decrease below 75°C transmittance. Compared to the tetrahedral site, the octahedral site is more significantly altered by variations in the synthesis temperature. This indicates that the sample's lattice strain changes octahedral which was said by Prasetya et al. (2025).

The $Zn_{0.5}Cu_{0.5}Fe_2O_4$ Nanoparticles has two absorption bands at tetrahedral site (550 and 700 cm^{-1}) and octahedral site (400-450 cm^{-1}) which confirms the existence of spinel ferrite structure with M-O bonds which was observed by Abuzeyad et al. (2024). The $NiFe_2O_4$ nanoparticles demonstrates with absorption between tetrahedral Fe-O stretching and octahedral M-O stretching. Where, the peaks for surface functional groups and absorbed water were also found by Hariharasuthan et al. (2022). The Cobalt ferrite nanoparticles show characteristic bands near 550-600 cm^{-1} and 350-400 cm^{-1} which is associated with M-O stretching as shown in **Figure 7(a)**. But when doped with Eu^{3+} it slightly shifts the bands to 600-650 $cm^{-1}$and 400-450 cm^{-1} due to altered lattice parameters was observed by Boddolla and Ravinder (2024) as shown in **Figure 7(b)**. Lakshmi et al. (2016) explained that according to Waldron's model, shorter Fe^{3+}-O^{2-} bonds and lower cation coordination (4 oxygens) lead to higher force constants and increased vibrational intensity, which is why the higher-frequency v_1 band (tetrahedral) seems stronger. Kumar et al. (2014) said that on the other hand, longer bonds, higher coordination (6 oxygens), and partly covalent nature reduce dipole moment shifts during vibration, resulting in the weaker v_2 band (octahedral). Therefore, this leads to the appearance of strong and weak absorption bands.

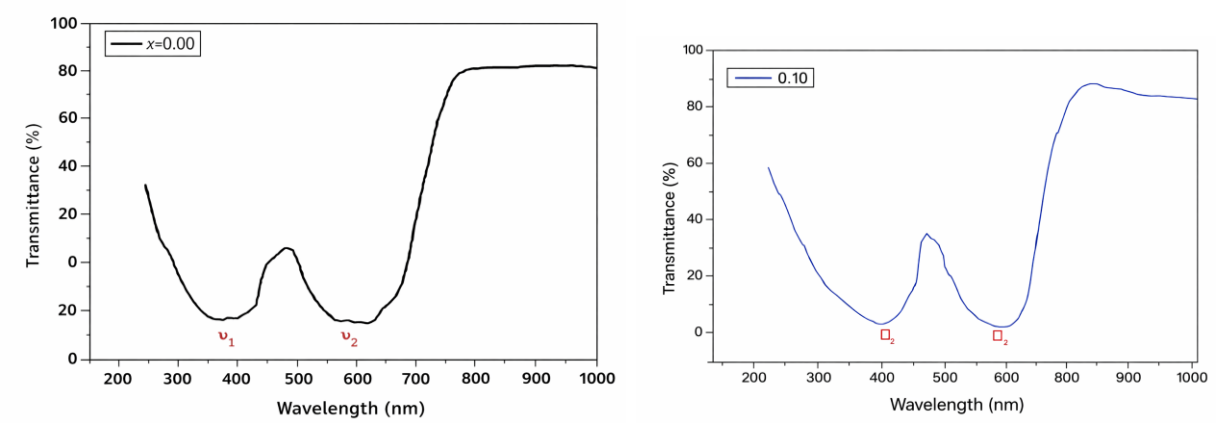

Figure 7. (a) Shows the FTIR spectrum of $CoEu_xFe_{2-x}O_4$ at x = 0.00 and (b) Shows the FTIR spectrum of $CoEu_xFe_{2-x}O_4$ at x = 0.10 (Boddolla and Ravinder, 2024).

Table 3. Higher frequency tetrahedral (v1) and lower frequency octahedral (v2) vibrational bands (cm^{-1}) for the synthesized ferrite compounds.

Ferrite compound	Tetrahedral band (cm^{-1})	Octahedral band (cm^{-1})	Reference
$ZnFe_2O_4$	540–550 cm^{-1}	455–470 cm^{-1}	Sagayaraj et al. (2017)
$CoFe_2O_4$	573 cm^{-1}	455 cm^{-1}	Sagayaraj et al. (2019b)
$Ni_{0.5M}Tb_{0.5M}Fe_2MO_4$/PVP	584–610 cm^{-1}	412–422 cm^{-1}	Sagayaraj et al. (2020)
$Zn_{0.5}Cu_{0.5}Fe_2O_4$	550 and 700 cm^{-1}	400-450 cm^{-1}	Abuzeyad et al. (2024)
GO-$CuFe_2O_4$	573 cm^{-1}	416 cm^{-1}	Hammoodi et al. (2024)
$NiFe_2O_4$	602 cm^{-1}	422 cm^{-1}	Hariharasuthan et al. (2022)
$ZnFe_2O_4$	573 and 580 cm^{-1}	436 and 443 cm^{-1}	Al-Wasidi Alreshaidan (2024)
$CoEu_xFe_{2-x}O_4$(x = 0.00,0.10)	550-600 cm−1(x=0.00) and 600-650 cm−1(x=0.10)	350-400 cm^{-1} (x=0.00) and 400-450 cm^{-1} (x=0.10)	Boddolla et al. (2024)
$Mn_xZn_{1-x}Fe_2O_4$ (x = 0.5, 0.6, 0.7)	600–500 cm^{-1}	450–350 cm^{-1}	Deepty et al. (2019)
NixZn1−xFe2O4 (x=0.5, 0.6, 0.7)	600–500 cm^{-1}	450–350 cm^{-1}	Srinivas et al. (2019)
$CoGd_{2x}Fe_{2-2x}O_4$ (x = 0.00, 0.05, 0.10, 0.15, 0.20, 0.25)	Around 550 cm^{-1}	Around 400 cm^{-1}	Farid et al. (2015)
$Ni_{0.5-x}Cd_xZn_{0.5}Fe_2O_4$ (x = 0, 0.15, 0.30)	570–597 cm^{-1}	418–420 cm^{-1}	Patil et al. (2017)
$Li_{0.5-x/2}Zn_xFe_{2.5-x/2}O_4$ (x = 0.0, 0.2, 0.4, 0.6, 0.8 and 1.0)	510 - 800 cm^{-1}	250 - 510 cm^{-1}	Rathod et al. (2017)
$MgSm_xFe_{2-x}O_4$ (x = 0,0.025, 0.050, 0.075, 0.100)	600 cm^{-1}	395 cm^{-1}	Venkatesh et al. (2021)
$KFe_{1-x}La_xO17$ (x =0, 0.02, 0.06 and 0.1)	468 $cm^{-1}$and 449 cm^{-1} (x = 0.02 and 0.06)	Below 400 cm^{-1}	Saeed et al. (2020)
$Ni_{0.2}Mg_{0.3}Zn_{0.5}Fe_2O_4$	560-566 cm^{-1}	430-461 cm^{-1}	Vidya et al. (2020)

3.3 Electron Microscopy (TEM and SEM)

Electron microscopy is a crucial technique for characterizing the morphology and size of nanoparticles, utilizing a beam of electrons to provide highly magnified images. Transmission Electron Microscopy (TEM) is particularly effective for determining particle shape and size, as seen in studies where $ZnFe_2O_4$ (Sagayaraj et al., 2017) and $CoFe_2O_4$ (Sagayaraj et al., 2019b) nanoparticles were confirmed to be spherical. As the particle size range is between 20 to 50 nm, it shows spherical shape as shown is **Figure 8**. An advanced version, High-Resolution TEM (HR-TEM), further revealed the high crystallinity and particle size range of 2-20 nm in Ce-doped $ZnFe_2O_4$ was reported by Prakash et al. (2022).

In contrast, Field Emission Scanning Electron Microscopy (FE-SEM) focuses on surface details, revealing a unique cauliflower-like morphology with pores and rough aggregates for Zn-doped $MnFe_2O_4$ said by Poongodi et al. (2024), a structure highly advantageous for applications like supercapacitors due to its high surface area. These findings collectively demonstrate the critical role of electron microscopy in linking a material's physical structure to its potential uses. When undoped $Fe^{2+}Al_2^{3+}O_4^{2-}$ samples FE-Sem image shows that it has large amount of pore with particle size ranging from 500 nm and 5µm. When Co^{2+} is doped with $Fe^{2+}Al_2^{3+}O_4^{2-}$ it seems that the pores slightly reduce was observed by Rodríguez et al. (2019). In Fe-Co-Al_2O_4 (600, 700, 800, 900, 1000ºC), there occurs increased agglomeration and reduced grain size as annealing temperature increases as shown in **Figure 9**. The particles range in size and shape from 20 to 100 nm at lower annealing temperatures (600, 700, and 800 ºC), but at higher temperatures (900 and 1000ºC), particles acquire irregular shape and range from 18.76 to 24.95 nm was reported by Poongodi et al. (2023). The densification and growth of smaller ferrite nanoparticles were greater than those of larger ones. The $Cu_{0.4M}Fe_{2.96M}O_4$ were annealed at 900°C, an agglomerated spongy and flaky like particles were gained as shown in **Figure 10**. Because the surface energy of the smaller nanoparticles is higher, there is more pressure for grain expansion and densification, which lowers the Gibbs energy of the system was observed by Sagayaraj et al. (2019c).

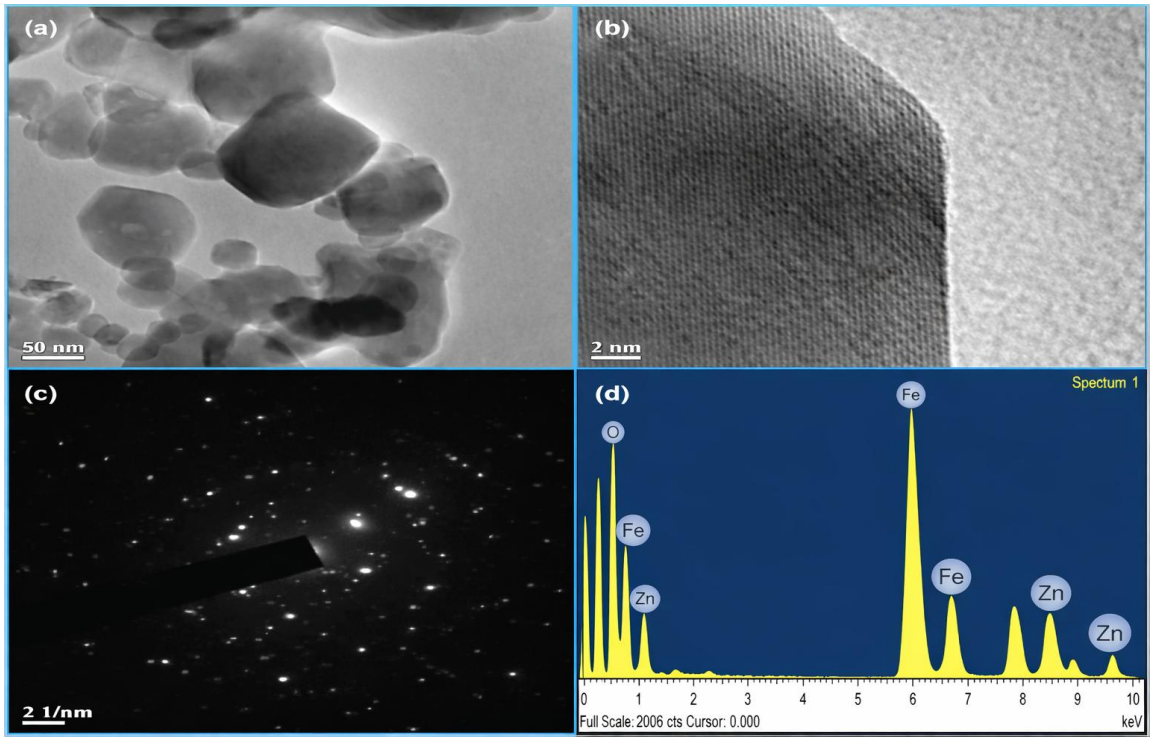

Figure 8. (a), (b) TEM images, (c) SAED pattern and (d) EDAX spectrum of $ZnxFe_2O_4$ (x = 0.03 M) nanoparticles (Sagayaraj et al., 2017).

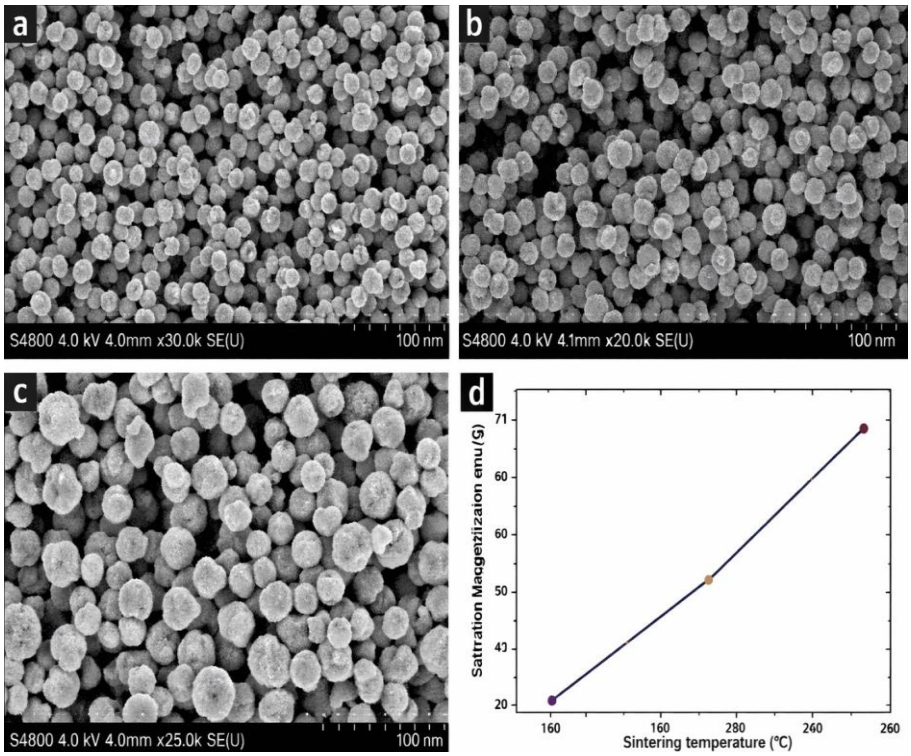

Figure 9. SEM images of $CoFe_2O_4$ solvothermal treated at (a) 160°C, (b) 180°C, and (c) 200°C for 16 hours along with (d) the saturation magnetization dependence on the sintering temperature (Rafienia et al., 2018).

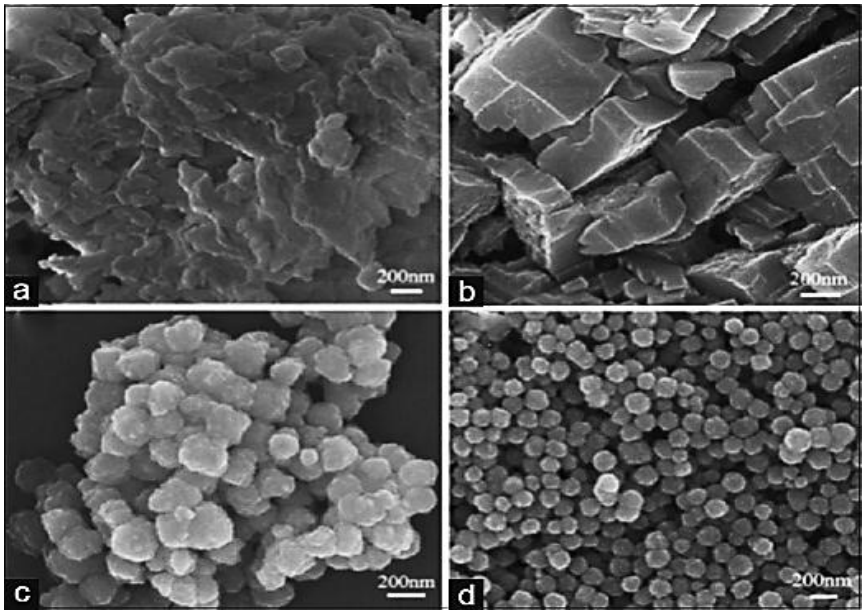

Figure 10. SEM images of $MgFe_2O_4$ materials taken at various time intervals of (a) 10 min, (b) 2 h, (c) 8 h, and (d) 11 h (Rafienia et al., 2018).

3.4 Vibrating Sample Magnetometry (VSM)

A vibrating sample magnetometer (VSM) is a crucial tool for characterizing the magnetic properties of materials. Studies on various nanoparticles highlight how different modifications affect their magnetic behaviour. As the applied field is increased to a positive value large enough to saturate the material's polarization, M (moments) is reduced to a negative value large enough to cause saturation in the opposite direction before being increased back to zero. This creates a symmetrical closed loop known as hysteresis. For instance, PVP-coated $ZnFe_2O_4$ nanoparticles demonstrate superparamagnetic behaviour with a high saturation magnetization (Ms) was observed by Sagayaraj et al. (2017) as shown in **Table 4**. The Curie temperature drops and magnetization rises as a result of the super-exchange interaction between the Fe^{3+} ions and the O^{2-} anions. This indicates that at lower temperatures, the material's magnetism is increased as discussed by Naeem et al. (2009). Doping also significantly alters these properties; doping Fe_3O_4 with Cobalt ions drastically increases the magnetic anisotropy constant, while increasing the non-magnetic Zn^{2+} content in $MgFe_2O_4$ decreases the Ms as in **Table 4**. Conversely, a small amount of Zinc doping in $MnFe_2O_4$ can surprisingly increase the Ms Accordingly, when Zn^{2+} is substituted with nickel, copper ferrite the saturation magnetisation decreases were reported by Sagayaraj et al. (2018). Due to single domain nature, demagnetisation occurs in highly coercive nanoparticles. In magnetic nanoparticles, coercivity is one of the most important measures.

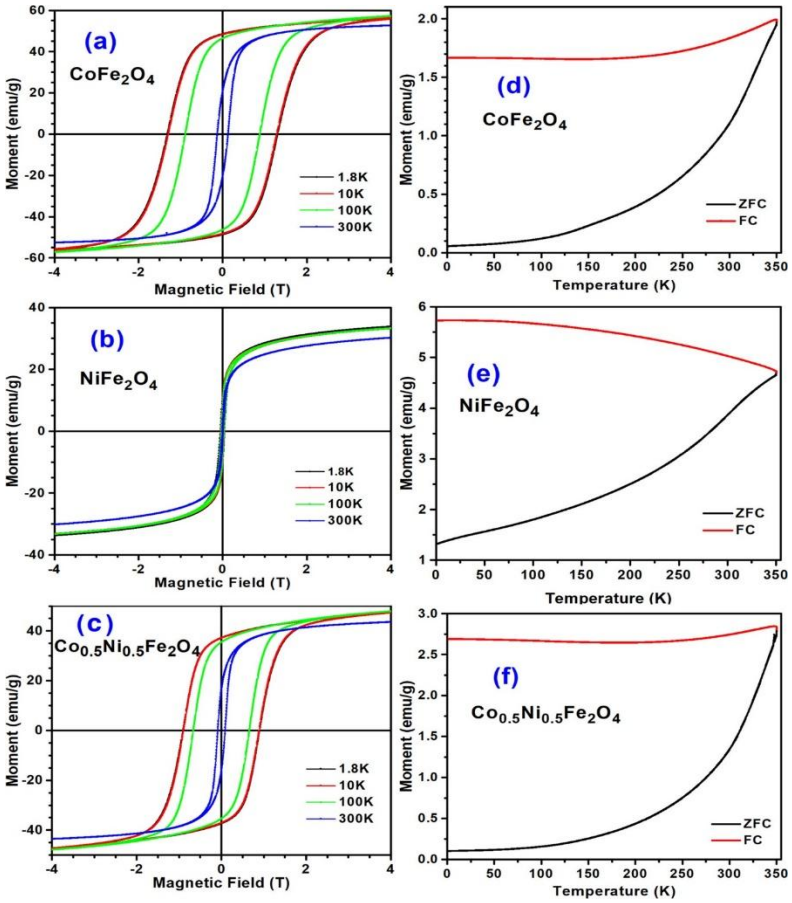

Figure 11. Figure showing (a, b, c) Magnetization (M) versus applied magnetic field (H) curves for $CoFe_2O_4$, $NiFe_2O_4$, and $Co_{0.5}Ni_{0.5}Fe_2O_4$NPs. (d, e, f) Temperature-dependent magnetization curves (M vs T) for the same samples (Ortiz et al., 2018).

Similarly, rare-earth doping with Cerium in $ZnFe_2O_4$ leads to a decrease in Ms as the Cerium content rises, which results in superparamagnetic behaviour as reported by Jayarajan et al. (2023). These examples show how precise control over doping and coating can tune the magnetic characteristics of nanomaterials for various applications. The Terbium substituted nickel ferrite exhibits ferrimagnetism with enhanced magnetic characteristics. Here the Ms value is slightly decreased compared to undoped nickel ferrite as shown in **Figure 11**. On Terbium substitution, the coercivity is increased which indicates higher magnetic anisotropy and improved magnetic hardness due to localised spin-orbit interaction (Sagayaraj et al., 2020). The $CoFe_2O_4$ shows ferrimagnetic behaviour, with higher saturation magnetisation. The coercivity was found to be slightly higher, suggesting moderate magnetic hardness and resistance to demagnetization under applied magnetic fields, which contributes to stability in biomedical applications was confessed by Arshad et al. (2021). As a result of Fe-Co-Al_2O_4 (600, 700, 800, 900, 1000 ºC) the increase in annealing temperature affects the coercivity, magnetic moment and Remnant ratio values of samples. Lower temperatures cause weaker magnetism with lower coercivity, magnetic moment, and Remnant ratio values because atoms are less able to move and reorient themselves. A stronger magnetization with greater coercivity, magnetic moment, and Remnant ratio values is the result of more atoms moving and reorienting themselves at higher temperatures as shown in **Table 4**. This explains why the annealing temperature affects these results was reported by (Poongodi et al., 2023).

Table 4. Magnetic properties of the ferrite compound, revealing saturation magnetization (Ms), remanent magnetization (Mr), coercivity (Hc), squareness ratio (S), and magnetic moment (η_B).

Ferrite compound	Ms (emu/g)	Mr (emu/g)	(Oe)	S = Mr/Ms	ηB	Reference
$ZnFe_2O_4$	23.451 emu/g	751.58 emu/g	210.03	32.0489	10.1×10−4T	Sagayaraj et al. (2017)
$CoFe_2O_4$	0.5008 emu/g	0.1908	661.04	0.3809		(Sagayaraj et al., 2019b)
$Ni_{0.5}Tb_{0.5}Fe_2O_4$	0.576 emu/g	0.139 emu/g	165.96 Oe	0.2413	1.05×10-4T	Sagayaraj et al. (2020)
$NiFe_2O_4$	48.63 emu/g	4.71 emu/g	77.70 Oe	0.09	-	Majid et al. (2021)
$NiFe_2O_4$	64.91 emu/g	8.72 emu/g	125.79 Oe	0.13	-	Majid et al. (2021)
$CoFe_2O_4$	50.61 emu/g	10.75 emu/g	159.8 Oe	0.212	-	Darwish et al. (2019)
$ZnCoFe_2O_4$	50.71 emu/g	10.71 emu/g	225 Oe	0.211	-	Darwish et al. (2019)
$CoFe_2O_4$	41.0 emu/g	-	2–5 Oe	-	-	Karaagac et al. (2019)
$NiFe_2O_4$	47.23 and 51.3 emu/g	-	250.8 and 153.62 Oe	-	-	Sivakumar et al. (2011)
$CoFe_2O_4$	75 to 127 emu/g	-	0.01to 0.0156 Oe	12.03 to 12.6	-	Arshad et al. (2021)
$CuFe_2O_4$	7.35 emu/g		245.5 Oe		-	Salavati-Niasari et al. (2012)
$CuFe_2O_4$	32.39 emu/g	11.64 emu/g	517.16 Oe	0.46	1.37×10-4T	Mulud et al. (2020)
$CoFe_2O_4$	23 to 63 emu/g	-	90 to 203 Oe	-	-	Senthil et al. (2018)
$ZnFe_2O_4$	1.72 emu/g and 1.92 emu/g	0.0003 emu/g and 0.0007 emu/g	-	-	-	Sinthiya et al. (2015)
$NiFe_2O_4$	48.75 to 60.87 emu/g	17.44 to 18.95 emu/g	112.62 to 177.55 Oe	-	-	Kooti and Sedeh (2013)
Fe-Co-Al_2O_4	82.19 to 45.42 emu/g	56.084 to 20.758 emu/g	873.02 to 391.75 Oe	0.4570 to 0.4113	0.0070 to 0.0025 T	Poongodi et al. (2023)

3.5 Electron Paramagnetic Resonance (EPR)

Electron Paramagnetic Resonance (EPR) spectroscopy is a technique that detects and analyses materials with unpaired electrons. It works similarly to Nuclear Magnetic Resonance (NMR) but focuses on the magnetic properties of electrons rather than atomic nuclei. In an external magnetic field, the unpaired

electrons align either with or against the field, creating two distinct energy levels. When the sample is exposed to microwave radiation, the electrons absorb energy and jump to the higher energy level. The EPR spectrometer measures this energy absorption, providing a spectrum that reveals detailed information about the electron's local environment. Electron Paramagnetic Resonance (EPR) spectroscopy provides valuable insights into the magnetic properties of materials by measuring the g-factor, a dimensionless value that relates an applied magnetic field to the energy of electron spin states. A g-factor of approximately 2.0023 is characteristic of a free electron, so any deviation indicates interactions with its local chemical environment. For example, in $MgFe_2O_4$ nanoparticles, an EPR spectrum with a g-factor of around 2.4 suggests a specific local magnetic environment caused by Mg^{2+} ions, which leads to superparamagnetic resonance behavior where small magnetic nanoparticles act as paramagnets with a very high magnetic moment at high temperatures. EPR can also confirm the magnetic coupling between unpaired electrons. In Co-doped ferrites, EPR analysis verified the ferromagnetic behavior of the composite by confirming that the spins of the unpaired electrons were strongly coupled and aligned. This demonstrates EPR's utility in characterizing a material's magnetic properties at an electronic level was concluded by Singh et al. (2020) For $MgFe_2O_4$ nanoparticles, EPR spectra confirmed superparamagnetic resonance due to the presence of Mg^{2+} ions, with a g-factor of approximately 2.4 was reported by Sagayaraj et al. (2018) as shown in **Figure 12**. In Co-doped ferrites, EPR analysis confirmed the ferromagnetic behavior of the composites was reported by Sagayaraj et al. (2019b).

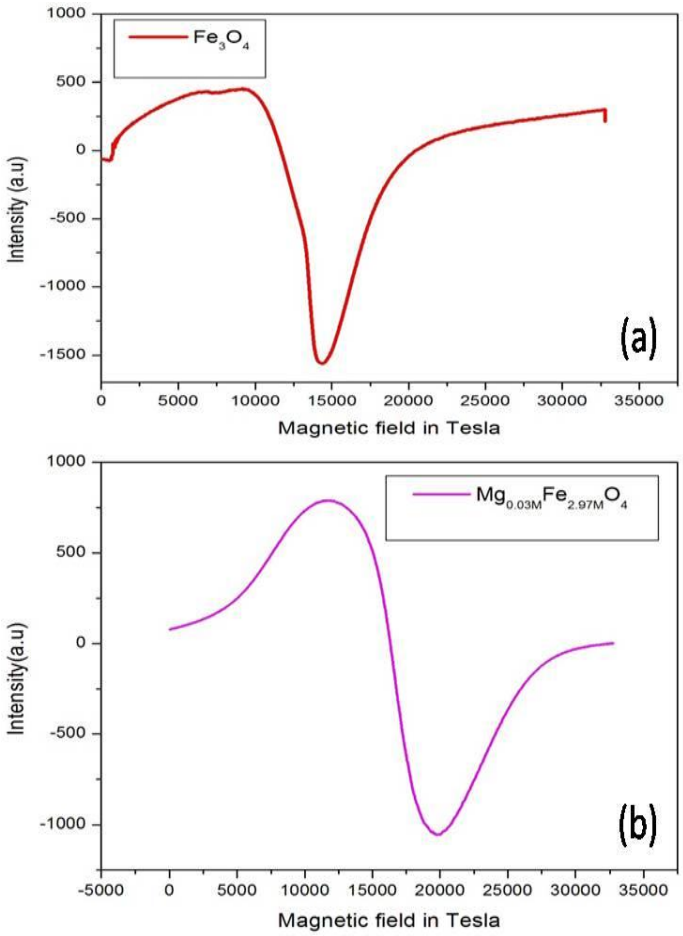

Figure 12. EPR image of $MgFe_2O_4$ nanoparticles (Sagayaraj et al., 2018).

4. Applications of Spinel Ferrite Nanoparticles

4.1 Biomedical Applications & Antibacterial Activity

Table 5 shows some properties of metal ferrite nanoparticles synthesized by microorganisms, including the effect of culturing temperature and their location within the cell. Spinel ferrites are emerging as effective antimicrobial agents. Studies on Ce-doped $ZnFe_2O_4$ have demonstrated significant antibacterial activity against both Gram-positive (Staphylococcus aureus, Bacillus cereus) and Gram-negative (Escherichia coli) bacteria as shown in **Figure 13**. The mechanism is attributed to the generation of reactive oxygen species (ROS) and the electrostatic interaction of positively charged metal ions (Ce^{3+}, Zn^{2+}, Fe^{3+}) with the negatively charged bacterial cell membrane, leading to cell wall disruption and death. Zones of inhibition were observed to be over 6 mm, confirming the efficacy of these nanoparticles was observed by Prakash et al. (2022). $Cu_{0.4M}Fe_{2.96M}O_4$ these materials' superparamagnetic behavior suggests that they hold tremendous potential for usage as materials in magnetic resonance imaging (MRI) applications said by Sagayaraj et al. (2018). Shewanellaoneidensis enhances magnetite biomineralization with active metabolism, resulting with high Fe^{2+} and pH conditions. The resultant biogenic magnetite has potential used in bioremediation and antimicrobial surfaces was discussed by Perez-Gonzalez et al. (2010).

The $Ni_xZn_{1-x}Fe_2O_4$ nanoparticles have antibacterial properties against Escherichia coli, Bacillus cereus, Staphylococcus citreus and Candida tropicalis. These nanoparticles have uses in wastewater treatment and antimicrobial coatings due to its magnetic durability and capacity to damage microbial cells observed by Martinson et al. (2022). Also, the $Mn_{1-x}Ce_xFe_2O_4$ nanoparticles were treated against Enterobacter cloacae, Escherichia coli, Staphylococcus haemolyticus and Staphylococcus petrasii subs. pragensis, Bacillussubtilis, Bacillus cereus under bacterial culturing temperature around 37 ºC. Their antibacterial activity was improved by changing surface reactivity and magnetic properties. This supports their use in medical device coating and infection prevention strategies was discovered by Prakash et al. (2022). The $CuFe_2O_4$ and $ZnFe_2O_4$ nanoparticle's antibacterial activity was evaluated against Escherichia coli (Gram-negative) and Staphylococcus aureus (Gram-positive). The **Figure 13**. shows clear inhibition zones surrounding the disks containing nanoparticles on the bacterial culture plates, indicating their potential to break bacterial cell membranes and kill both Gram-positive and Gram-negative pathogens observed by Kahkesh et al. (2023). Along with this, the **Table 5**, represents some other ferrite nanoparticles showing antibacterial activities.

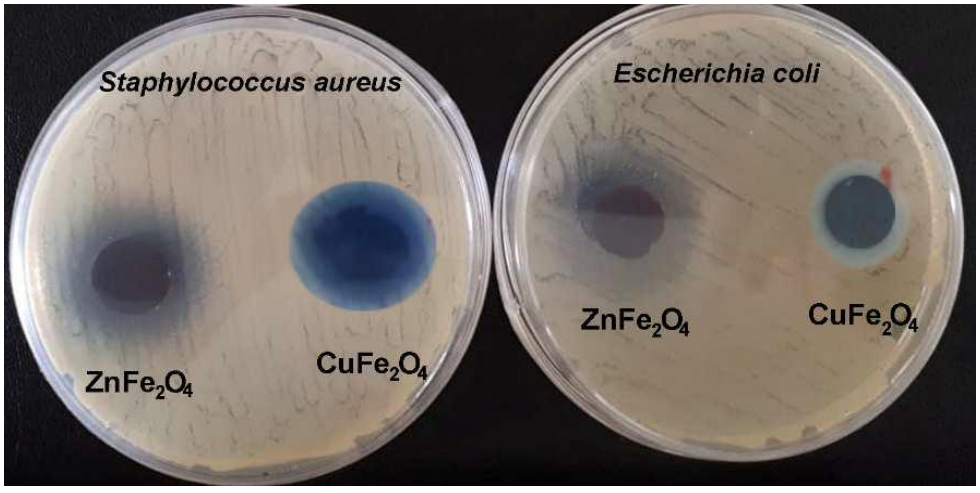

Figure 13. Antibacterial activity of $CuFe_2O_4$ and $ZnFe_2O_4$ against Escherichia coli and staphylococcus aureus (Kahkesh et al., 2023).

Table 5. Properties of ferrite nanoparticles synthesized by microorganisms, including the effect of culturing temperature and their location within the cell.

Compound	Microorganisms	Culturing temperature	Particle Size (nm)	Location	References
Fe_3O_4	Shewanellaoneidensis	28 ºC	40–50	Extracellular	Perez- Gonzalez et al. (2010)
Ferrous hydroxide	Recombinant AMB-1	28 ºC	20	Intracellular	Amemiya et al. (2007)
Fe_3O_4	Yeast cells	36 ºC	Not available	Extracellular	Zhou et al. (2009a)
$FePO_4$	Yeast cell	36 ºC	Not available	Extracellular	Zhou et al. (2009b)
Fe (III)-oxide	Shewanella oneidensis MR-1	25 ºC	30–43	Intracellular	Bose et al. (2009)
$CoFe_2O_4$	Phanerochaete chrysosporium	28 ºC	11.5 nm	Cellular medium	Oprica et al. (2015)
$NixZn_{1-x}Fe_2O_4$	Escherichia coli, Bacillus cereus, Staphylococcus citreus, Candida tropicalis		35.1 nm		Martinson et al. (2022)
$CoFe_2O_4$	Monascus purpureus	30 ºC	8.00 nm	Extracellular	El Sayed et al. (2020)
$Mn_{1-x}Ce_xFe_2O_4$	Enterobacter cloacae, Escherichia coli, Staphylococcus haemolyticus and Staphylococcus petrasii subs. pragensis, Bacillussubtilis, Bacillus cereus	37 ºC	17 to 20 nm	Intracellular	Prakash et al. (2022)
$CuFe_2O_4$, $ZnFe_2O_4$ and $MnFe_2O_4$	S. aureus and E. coli		~25 nm	cellular	Dabagh et al. (2023)
$CuCr_xFe_{2-x}O_4$	E. coli	37 °C	43.3–20.2 nm	Intracellular	Ansari et al. (2018)
$Li_{0.25}Ni_{0.5}Er_xFe_{2.25-x}O_4$	Campylobacter jejuni, Enteropathogenic E. coli, Vibrio cholerae and Listeria monocytogenes, Staphylococcus aureus	37°C	24 nm to107 nm		Noreen et al. (2017)
$CuFe_2O_4$ and $ZnFe_2O_4$	Escherichia coli and Staphylococcus aureus	37˚C	20 and 40 nm		Kahkesh et al. (2023)
$Cu_{1-x}Ag_xFe_2O_4$	S. aureus, B. subtilis and E. faecalis, P. aeruginosa, E. coli and K. pneumoniae	37 °C	11 to 13nm		Gomes et al. (2018)
$Mn_{0.5}Cu_{0.5}Er_xFe_{2-x}O_4$	Bacillus cereus, Staphylococcus aureus, Pseudomonas aeruginosa, Fusarium oxysporum, Aspergillus flavus, A. terreus, A. fumigatus, A. niger, and Rhizopus sp.,	37 °C	59.58 to 39.16 nm		Abu et al. (2025)

4.2 Magneto-dielectric and Electrochemical Applications

The unique combination of magnetic and electrical properties makes spinel ferrites suitable for electronic applications. The research into doped ferrite materials reveals several key findings. Studies on Zn-doped $MgFe_2O_4$ have demonstrated intriguing magneto-dielectric properties, where the dielectric constant can be manipulated by an external magnetic field, showing a positive magneto-dielectric constant up to 2000 Oe before decreasing. This suggests potential for applications in tunable electronic devices. Furthermore, the electrical properties are significantly affected by doping, as seen in Ce-doped $ZnFe_2O_4$, which exhibited a lower charge-transfer resistance of 2400 Ω compared to the 2600 Ω of pure $ZnFe_2O_4$, thereby enhancing its

electrical conductivity. The application of these materials extends to energy storage, with Zn-doped $MnFe_2O_4$ showing considerable promise as an electrode for supercapacitors, achieving a specific capacitance of 53.518 Fg^{-1} at a scan rate of 30 mVs^{-1}. These findings collectively highlight the diverse and useful properties that can be engineered in ferrite materials through strategic doping. Accordingly, with its large dielectric constant, low dielectric loss, and high resistivity, the Al-substituted cobalt ferrite shows promise for use in electrical and high-frequency devices was discovered by Priya et al. (2019).

4.3 Photocatalytic Application

Recent study has shown that ferrite nanoparticles are effective photocatalysts due to their magnetic and electronic properties, particularly for wastewater treatment and dye degradation. These particles are magnetically recoverable, making them promising for practical applications in catalysis and ecological restoration. Among them Aluminium doped Cobalt ferrite ($CoAl_xFe_{2-x}O_4$) exhibits effective degradation of methylene blue under visible light, due to its enhanced charge separation and decreased recombination, where the synthesised nano particles are used in wastewater treatment was concluded by Abbas et al. (2020). Then $Mg_{0.5}Zn_{0.5-x}Ni_xFe_2O_4$ demonstrates higher photocatalytic activity for dye degradation and have potential uses in high-frequency electronics and also it explores the purification of contaminated water with different pollutants confessed by Sharma et al. (2018). The $ZnFe_2O_4$ nanoparticles were observed to have a narrow visible band gap approximately 2.01 eV, which allows them to quickly absorb sunlight and create electron-hole pair for catalysis. They have obtained 99% degradation of methylene blue in 60 minutes using the collected sunlight. At 600ºC annealing, the $ZnFe_2O_4$ nanoparticle's optimal size, surface area and crystallinity enables dye absorption and charge separation, which reduces recombination and improves photocatalytic efficiency said by Yadav et al. (2018a).

Also, the Rare-Earth doped Ferrites plays a crucial role in enhancing the photocatalytic performance. Among them incorporation of La, Nd, Gd, Y, Bi etc. in the lattice of ferrite nanoparticles provides enhanced photocatalytic degradation of pollutants. Which is due to changes in structural, optical, and electrical features, such as increased visible-light absorption etc. The $La_xMnFe_{2-x}O_4$ shows enhanced optical and electrical features leading to superior dye degradation was said by Baig et al. (2020). Tailored band structures of $BiFeO_3$ exhibit excellent stability and efficiency for pollutant elimination was observed by Golizadeh and Hosseini (2024). The rapid regeneration, reusability, and low treatment cost of spinel ferrite nanocomposites make them popular for water purification. By producing electron–hole pairs, their small band gap (< 3 eV) permits effective photocatalytic activity in the presence of sunlight. Highly oxidative hydroxyl radicals are created when photogenerated holes combine with water molecules to break down organic contaminants. Conduction band electrons simultaneously create hydroperoxyl and superoxide radicals, which accelerates the breakdown of pollutants as (Ahmad et al., 2023) shown in **Figure 14**. Cobalt ferrite nanoparticles have small band gap in the visible area, but their photocatalytic activity is limited under low-power visible light, due to electron-hole recombination. Adding H_2O_2 reduces recombination by producing reactive hydroxyl radicals, increasing efficiency. As a result, more than 90% of methylene blue and methyl orange colours decay within 90 minutes was observed by Ahmad et al. (2023). The $Co_{0.5}Sr_{0.5}La_{0.06}Fe_{1.94}O_4$ and $Co_{0.5}Sr_{0.5}Nd_{0.06}Fe_{1.94}O_4$ nanoparticles causes considerable improvements in structural and photocatalytic features, especially for textile dyes. Also, the rare earth ions enhance visible light absorption and charge separation, improving the catalytic performance for wastewater treatment was explained by Venkatesh et al. (2023). The Yttrium substituted Co-Mg ferrite nanoparticles improved their dielectric, optical and photocatalytic performance. These properties make the material more successful in photodegrading dyes, which indicates their potential in water purification and environmental cleanliness was reported by Mohammed and Basfer (2022). Thus, these properties are shown in **Table 6**.

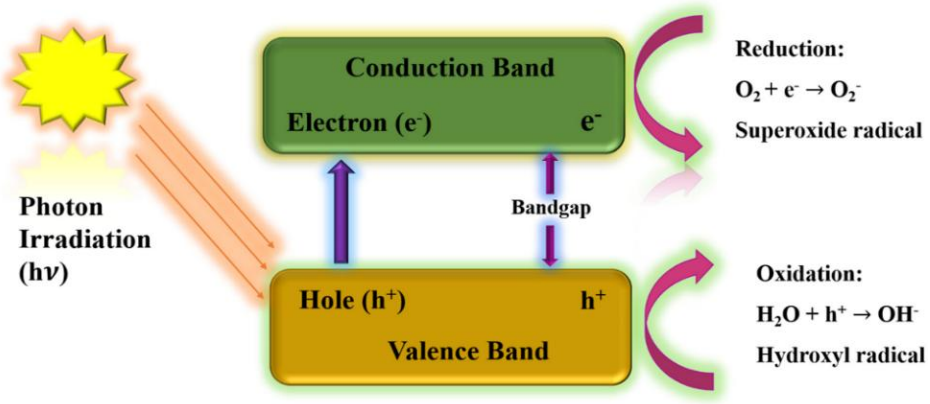

Figure 14. Photocatalytic degradation is depicted during sunlight (Ahmad et al., 2023).

Table 6. Photocatalytic application of Ferrite nanoparticles using various pollutant under specific light source.

Ferrite compound	Pollutant	Light source	Degradation	Dye conc. (mg/L)	Reference
$CoAl_xFe_{2-x}O_4$	Methylene Blue Dye	Visible light bulbs	10–15%	10	Abbas et al. (2020)
$Mg_{0.5}Zn_{0.5-x}Ni_xFe_2O_4$	Methylene blue	Direct Sunlight	36.94%	5	Sharma et al. (2018)
$ZnFe_2O_4$	methylene blue	Natural sunlight	74 - 99 %	10	Yadav et al. (2018a)
$La_xMnFe_{2-x}O_4$	Crystal violet (CV) dye	Incandescent filament (lamp)	95%		Baig et al. (2020)
$BiFeO_3$, $Bi_{0.9}Gd_{0.1}FeO_3$, $Bi_{0.9}Tb_{0.1}FeO_3$, $Bi_{0.9}Dy_{0.1}FeO_3$, $Bi_{0.9}Ho_{0.1}FeO_3$, and $Bi_{0.9}Er_{0.1}FeO_3$	Methylene blue	Simulated solar light	37-77%	10	Gholizadeh and Hosseini (2024)
$Co_{0.5}Sr_{0.5}La_{0.06}Fe_{1.94}O_4$, $Co_{0.5}Sr_{0.5}Nd_{0.06}Fe_{1.94}O_4$	CR and RhB	sunlight	61 and 67%	10	Ahmad et al. (2023)
$CoFe_2O_4/H_2O_2$	Methyl Orange, MB mixture	Visible LED light	90%	90	Prajapati et al. (2025)
$CoFe_2O_4$	RhB	Visible (Halide lamp)	73%	10	Sundararajan et al. (2017)
$MgGd_xFe_{2-x}O_4$	Methylene blue	Photo light irradiation			Venkatesh et al. (2023)
$Co_{0.7}Mg_{0.3}Y_xFe_{2-x}O_4$	Methylene blue	Xenon lamp	5.81%	5	Mohammed and Basfer (2022)

5. Conclusion

Spinel ferrites represent a highly versatile class of magnetic materials, and their unique properties, which are heavily dependent on their nanostructure, have made them indispensable in various high-tech applications. The ability to precisely control their synthesis and characterization is paramount to their continued development. As this review has demonstrated, a diverse array of fabrication techniques from cost-effective co-precipitation to advanced hydrothermal and sol-gel methods provides researchers with the necessary tools to tailor these materials for specific functionalities. Each method offers a unique trade-off between cost, complexity, and the final material's quality, such as particle size, morphology, and crystallinity. Characterization techniques, including XRD, FTIR, and electron microscopy (TEM/SEM), are essential for linking these synthesis parameters to the material's structural attributes. The data presented here show a clear correlation between factors like calcination temperature, pH, and the presence of surfactants, and the resulting crystallite size, lattice constant, and overall morphology. The magnetic

properties, measured by techniques like VSM, are also highly dependent on these structural characteristics and the distribution of cations within the spinel lattice. The superparamagnetic behavior and high saturation magnetization of these nanoparticles make them especially promising for biomedical applications, while their tailored magnetic responses are ideal for high-frequency electronics. So, the field of spinel ferrite nanotechnology is a dynamic area of research driven by the synergy between controlled synthesis and sophisticated characterization. Continued exploration of novel doping strategies, hybrid materials, and scalable synthesis methods will undoubtedly unlock further potential for these remarkable materials, paving the way for innovations in electronics, medicine, and energy.

Conflicts of Interest

The author has no conflict of interest.

Acknowledgments

The authors gratefully acknowledge Adhi College of Engineering and Technology and St. Joseph's College of Arts and Science (Autonomous) for providing access to its library resources. These facilities were crucial for the successful conduct of this research.

AI Disclosure

We declare that no assistance is taken from generative AI to write this article.

References

Abbas, N., Rubab, N., Sadiq, N., Manzoor, S., Khan, M.I., Garcia, J.F., Aragao, I.B., Tariq, M., Akhtar, Z., & Yasmin, G. (2020). Aluminum-doped cobalt ferrite as an efficient photocatalyst for the abatement of methylene blue. Water, *12*(8), 2285. https://doi.org/10.3390/w12082285.

Abu-Elsaad, N.I., Metwally, R.A., & Nawara, A.S. (2025). Erbium substituted Mn-Cu ferrite nanoparticles: synthesis, structural, magnetic, and antimicrobial activity properties. *Brazilian Journal of Physics*, *55*(4), 165. https://doi.org/10.1007/s13538-025-01784-z.

Abuzeyad, O.H., El-Khawaga, A.M., Tantawy, H., Gobara, M., & Elsayed, M.A. (2024). Photocatalytic degradation of methylene blue dye by promising zinc copper ferrite nanoparticles for wastewater treatment. *Journal of Inorganic and Organometallic Polymers and Materials*, *34*(6), 2705-2715. https://doi.org/10.1007/s10904-024-03006-6.

Ahlawat, A., Sathe, V.G., Reddy, V.R., & Gupta, A. (2011). Mossbauer, Raman and X-ray diffraction studies of superparamagnetic $NiFe_2O_4$ nanoparticles prepared by sol–gel auto-combustion method. *Journal of Magnetism and Magnetic Materials*, *323*(15), 2049-2054.

Ahmad, I., Safdar, M., Yasmin, N., Iftikhar, A., Kalsoom, A., Khalid, S., & Mirza, M. (2023). Rare earth ions (La^{3+}, Nd^{3+}) substituted cobalt–strontium spinel ferrites for photocatalytic degradation of textile dyes. *Water Practice & Technology*, *18*(8), 1742-1755.

Al Kiey, S.A., Ramadan, R., & El-Masry, M.M. (2022). Synthesis and characterization of mixed ternary transition metal ferrite nanoparticles comprising cobalt, copper and binary cobalt–copper for high-performance supercapacitor applications. *Applied Physics A*, *128*(6), 473. https://doi.org/10.1007/s00339-022-05590-1.

Al-Wasidi, A.S., & Alreshaidan, S.B. (2024). Enhanced removal of rhodamine b Dye from aqueous media via adsorption on facilely synthesized zinc ferrite nanoparticles. *Inorganics*, *2*(7), 191. https://doi.org/10.3390/inorganics12070191.

Amemiya, Y., Arakaki, A., Staniland, S.S., Tanaka, T., & Matsunaga, T. (2007). Controlled formation of magnetite crystal by partial oxidation of ferrous hydroxide in the presence of recombinant magnetotactic bacterial protein Mms6. *Biomaterials*, *28*(35), 5381-5389.

Ansari, M.A., Baykal, A., Asiri, S., & Rehman, S. (2018). Synthesis and characterization of antibacterial activity of spinel chromium-substituted copper ferrite nanoparticles for biomedical application. *Journal of Inorganic and Organometallic Polymers and Materials*, *28*(6), 2316-2327.

Arcaro, S., & Venturini, J. (2021). Magnetic, electrical, and optical properties of ferrites. In: Arcaro, S., & Venturini, J. (eds) *Modern Ferrites in Engineering: Topics in Mining, Metallurgy and Materials Engineering* (pp. 25-47). Springer International Publishing. https://doi.org/10.1007/978-3-030-78988-6_3.

Arshad, J.M., Raza, W., Amin, N., Nadeem, K., Arshad, M.I., & Khan, M.A. (2021). Synthesis and characterization of cobalt ferrites as MRI contrast agent. *Materials Today: Proceedings*, *47*, S50-S54. https://doi.org/10.1016/j.matpr.2020.04.746.

Baig, M.M., Zulfiqar, S., Yousuf, M.A., Touqeer, M., Ullah, S., Agboola, P., Warsi, M.F., & Shakir, I. (2020). Structural and photocatalytic properties of new rare earth La^{3+} substituted $MnFe_2O_4$ ferrite nanoparticles. *Ceramics International*, *46*(14), 23208-23217. https://doi.org/10.1016/j.ceramint.2020.06.103.

Bao, C., Serrano-Lotina, A., Niu, M., Portela, R., Li, Y., Lim, K.H., Liu, P., Wang, W.J., Bañares, M.A., & Wang, Q. (2023). Microwave-associated chemistry in environmental catalysis for air pollution remediation: a review. *Chemical Engineering Journal*, *466*, 142902. https://doi.org/10.1016/j.cej.2023.142902.

Boddolla, S., & Ravinder, D. (2024). Eu3+ Doped CoFe2O4 nanoparticles with XRD and FTIR analysis. *Journal for Research in Applied Sciences and Biotechnology*, *3*(2), 135-138.

Bose, S., Hochella Jr, M.F., Gorby, Y.A., Kennedy, D.W., McCready, D.E., Madden, A.S., & Lower, B.H. (2009). Bioreduction of hematite nanoparticles by the dissimilatory iron reducing bacterium Shewanella oneidensis MR-1. *Geochimica et Cosmochimica Acta*, *73*(4), 962-976.

Chandra, G., Srivastava, R.C., Reddy, V.R., & Agrawal, H.M. (2017). Effect of sintering temperature on magnetization and Mössbauer parameters of cobalt ferrite nanoparticles. *Journal of Magnetism and Magnetic Materials*, *427*, 225-229.

Dabagh, S., Haris, S.A., & Ertas, Y.N. (2023). Synthesis, characterization and potent antibacterial activity of metal-substituted spinel ferrite nanoparticles. *Journal of Cluster Science*, *34*(4), 2067-2078.

Darwish, M.S., Kim, H., Lee, H., Ryu, C., Lee, J.Y., & Yoon, J. (2019). Synthesis of magnetic ferrite nanoparticles with high hyperthermia performance via a controlled co-precipitation method. *Nanomaterials*, *9*(8), 1176. https://doi.org/10.3390/nano9081176.

Deepty, M., Srinivas, C., Kumar, E.R., Mohan, N.K., Prajapat, C.L., Rao, T.C., Meena, S.S., Verma, A.K., & Sastry, D.L. (2019). XRD, EDX, FTIR and ESR spectroscopic studies of co-precipitated Mn–substituted Zn–ferrite nanoparticles. *Ceramics International*, *45*(6), 8037-8044. https://doi.org/10.1016/j.ceramint.2019.01.029.

Dippong, T., Levei, E.A., & Cadar, O. (2021). Recent advances in synthesis and applications of MFe2O4 (M= Co, Cu, Mn, Ni, Zn) nanoparticles. *Nanomaterials*, *11*(6), 1560. https://doi.org/10.3390/nano11061560.

El-Sayed, E.S.R., Abdelhakim, H.K., & Zakaria, Z. (2020). Extracellular biosynthesis of cobalt ferrite nanoparticles by Monascus purpureus and their antioxidant, anticancer and antimicrobial activities: yield enhancement by gamma irradiation. *Materials Science and Engineering: C*, *107*, 110318. https://doi.org/10.1016/j.msec.2019.110318.

Farid, M., Ahmad, I., Aman, S., Kanwal, M., Murtaza, G., Alia, I., & Ishfaq, M. (2015). SEM, FTIR and dielectric properties of cobalt substituted spinel ferrites. *Journal of Ovonic Research*, *11*(1), 1-10.

Gholizadeh, A., & Hosseini, S. (2024). Effect of heavy rare-earth substitution on physical properties of $BiFeO_3$ thin films and their photocatalytic application. *Journal of the American Ceramic Society*, *107*(6), 4209-4222. https://doi.org/10.1111/jace.19729.

Gomes, G.A., da Costa, G.L., & da Silva Figueiredo, A.B.H. (2018). Synthesis of ferrite nanoparticles $Cu_{1-x}Ag_xFe_2O_4$ and evaluation of potential antibacterial activity. *Journal of Materials Research and Technology*, *7*(3), 381-386.

Gomes, J.A., Sousa, M.H., Tourinho, F.A., Mestnik-Filho, J., Itri, R., & Depeyrot, J. (2005). Rietveld structure refinement of the cation distribution in ferrite fine particles studied by X-ray powder diffraction. *Journal of Magnetism and Magnetic Materials*, *289*, 184-187.

Granone, L.I., Ulpe, A.C., Robben, L., Klimke, S., Jahns, M., Renz, F., Gesing, T.M., Bredow, T., Dillert, R., & Bahnemann, D.W. (2018). Effect of the degree of inversion on optical properties of spinel $ZnFe_2O_4$. *Physical Chemistry Chemical Physics*, *20*, 28267-28278.

Gupta, M., Das, A., Mohapatra, S., Das, D., & Datta, A. (2020). Surfactant based synthesis and magnetic studies of cobalt ferrite. *Applied Physics A*, *126*(8), 660. https://doi.org/10.1007/s00339-020-03823-9.

Hajalilou, A., & Mazlan, S.A. (2016). A review on preparation techniques for synthesis of nanocrystalline soft magnetic ferrites and investigation on the effects of microstructure features on magnetic properties. *Applied Physics A*, *122*(7), 680. https://doi.org/10.1007/s00339-016-0217-2.

Hammoodi, O.G., Mohammed, I.K., Majeed, A.H., Alheety, M.A., Mohammed, L.A., & Yahya, M.Z.A. (2024). Enhanced hydrogen storage capacity of graphene oxide through doping with copper ferrite nanoparticles. *Energy Storage*, *6*(1), e574. https://doi.org/10.1002/est2.574.

Hariharasuthan, R., Chitradevi, S., Radha, K.S., & Chithambaram, V. (2022). Characterization of NiFe2O4 (Nickel Ferrite) nanoparticles with very low magnetic saturation synthesized via co-precipitation method. *Applied Physics A*, *128*(12), 1045. https://doi.org/10.1007/s00339-022-06163-y.

Hemingway, B.S. (1990). Thermodynamic properties for bunsenite, NiO, magnetite, Fe_3O_4, and hematite, Fe_2O_3, with comments on selected oxygen buffer reactions. *American Mineralogist*, *75*(7-8), 781-790.

Herzer, G. (1990). Grain size dependence of coercivity and permeability in nanocrystalline ferromagnets. *IEEE Transactions on Magnetics*, *26*(5), 1397-1402.

Jayarajan, D., Sagayaraj, R., Silvan, S., Sebastian, S., Nithya, R., & Sujeetha, S. (2023). Green synthesis, structural and magnetic properties of $Mg_{0.5}Zn_{0.5}Fe_2O_4$ ferrite nanoparticles by the coprecipitation method: averrhoa bilimbi fruit. *Chemistry Africa*, *6*(4), 1875-1885.

Kahkesh, K.H., Baghbantaraghdari, Z., Jamaledin, D., Moghaddam, F.D., Kaneko, N., & Ghovvati, M. (2023). Synthesis, characterization, antioxidant and antibacterial activities of zinc ferrite and copper ferrite nanoparticles. *Materials Chemistry Horizons*, *2*(1), 49-56.

Kanagesan, S., Hashim, M., AB Aziz, S., Ismail, I., Tamilselvan, S., Alitheen, N.B., Swamy, M.K., & Rao, B.P.C. (2016). Evaluation of antioxidant and cytotoxicity activities of copper ferrite ($CuFe_2O_4$) and zinc ferrite ($ZnFe_2O_4$) nanoparticles synthesized by sol-gel self-combustion method. *Applied Sciences*, *6*(9), 184. https://doi.org/10.3390/app6090184.

Karaagac, O., Yildiz, B.B., & Köçkar, H. (2019). The influence of synthesis parameters on one-step synthesized superparamagnetic cobalt ferrite nanoparticles with high saturation magnetization. *Journal of Magnetism and Magnetic Materials*, *473*, 262-267.

Kaur, N., & Kaur, M. (2014). Comparative studies on impact of synthesis methods on structural and magnetic properties of magnesium ferrite nanoparticles. *Processing and Application of Ceramics*, *8*(3), 137-143. https://doi.org/10.2298/PAC1403137K.

Khan, H., Balouch, A., Soomro, K.F., Shaikh, H., Naz, S., Kandhro, A.A., Samejo, M.Q., & Memon, N.N. (2019). Effective heterogeneous photocatalytic degradation of crystal violet dye using manganese ferrite nanoparticles. *Pakistan Journal of Analytical & Environmental Chemistry*, *20*(1), 32-38.

Khanna, L., & Verma, N.K. (2013). Synthesis, characterization and in vitro cytotoxicity study of calcium ferrite nanoparticles. *Materials Science in Semiconductor Processing*, *16*, 1842-1848. https://doi.org/10.1016/j.mssp.2013.07.016.

Khishigdemberel, I., Uyanga, E., Hirazawa, H., &Sangaa, D. (2018). Influence of Cu dope on the structural behavior of $MgFe_2O_4$ at various temperatures. *Physica B: Condensed Matter*, *544*, 73-78. https://doi.org/10.1016/j.physb.2018.05.032.

Kooti, M., & Sedeh, A.N. (2013). Synthesis and characterization of $NiFe_2O_4$ magnetic nanoparticles by combustion method. *Journal of Materials Science & Technology*, *29*(1), 34-38.

Kumar, H., Singh, J.P., Srivastava, R.C., Negi, P., Agrawal, H.M., & Asokan, K. (2014). FTIR and electrical study of dysprosium doped cobalt ferrite nanoparticles. *Journal of Nanoscience, 2014*(1), 862415. https://doi.org/10.1155/2014/862415.

Lakshmi, M., Kumar, K.V., & Thyagarajan, K. (2016). Structural and magnetic properties of Cr-Co nanoferrite particles. *Advances in nanoparticles*, *5*(1), 103-113.

Layek, S., & Verma, H.C. (2015). Magnetic and dielectric properties of multiferroic $BiFeO_3$ nanoparticles synthesized by a novel citrate combustion method. *arXiv preprint arXiv:1502.05797.*

Liu, S., Feng, L., Xu, N., Chen, Z., & Wang, X. (2012). Magnetic nickel ferrite as a heterogeneous photo-Fenton catalyst for the degradation of rhodamine B in the presence of oxalic acid. *Chemical Engineering Journal*, *203*, 432-439.

Lu, H.F., Hong, R.Y., & Li, H.Z. (2011). Influence of surfactants on co-precipitation synthesis of strontium ferrite. *Journal of Alloys and Compounds*, *509*(41), 10127-10131.

Maji, N., & Dosanjh, H.S. (2023). Ferrite nanoparticles as catalysts in organic reactions: a mini review. *Magnetochemistry*, *9*(6), 156. https://doi.org/10.3390/magnetochemistry9060156.

Majid, F., Rauf, J., Ata, S., Bibi, I., Malik, A., Ibrahim, S.M., Ali, A., & Iqbal, M. (2021). Synthesis and characterization of $NiFe_2O_4$ ferrite: Sol–gel and hydrothermal synthesis routes effect on magnetic, structural and dielectric characteristics. *Materials Chemistry and Physics*, *258*, 123888. https://doi.org/10.1016/j.matchemphys.2020.123888.

Martinson, K.D., Beliaeva, A.D., Sakhno, D.D., Beliaeva, I.D., Belyak, V.E., Nianikova, G.G., & Popkov, V.I. (2022). Synthesis, structure, and antimicrobial performance of NixZn1− xFe2O4 (x= 0, 0.3, 0.7, 1.0) magnetic powders toward E. coli, B. cereus, S. citreus, and C. tropicalis. *Water*, *14*(3), 454. https://doi.org/10.3390/w14030454.

Mary, A.J., Manikandan, A., Chinnaraj, K., Arul Antony, S., & Neeraja, P. (2015). Comparative studies of spinel MnFe2O4 nanostructures: structural, morphological, optical, magnetic and catalytic properties. *Journal of Nanoscience and Nanotechnology*, *15*(12), 9732-9740. https://doi.org/10.1166/jnn.2015.10343.

Maurya, I., & Jayasimhadri, M. (2024). Comprehensive study on thermal, structural, and luminescent properties of BiYWO6: Eu3+ phosphors synthesized by various methods. *Journal of Materials Science: Materials in Electronics*, *35*(33), 2106. https://doi.org/10.1007/s10854-024-13852-2.

Melo, R.S., Banerjee, P., & Franco Jr, A. (2018). Hydrothermal synthesis of nickel doped cobalt ferrite nanoparticles: optical and magnetic properties. J*ournal of Materials Science: Materials in Electronics*, *29*(17), 14657-14667.

Mohammed, A.I., & Basfer, N.M. (2022). Improvement of dielectric, optical, and photocatalytic properties of rare earth (Y) substituted Co− Mg nanoferrites. *Journal of Materials Science: Materials in Electronics*, *33*(27), 21647-21659.

Moreno-Castilla, C., López-Ramón, M.V., Fontecha-Cámara, M.Á., Álvarez, M.A., & Mateus, L. (2019). Removal of phenolic compounds from water using copper ferrite nanosphere composites as fenton catalysts. *Nanomaterials*, *9*(6), 901. https://doi.org/10.3390/nano9060901.

Mulud, F.H., Dahham, N.A., & Waheed, I.F. (2020). Synthesis and characterization of copper ferrite nanoparticles. In *IOP Conference Series: Materials Science and Engineering* (Vol. 928, No. 7, p. 072125). IOP Publishing. Iraq.

Mushtaq, M.W., Shahbaz, M., Naeem, R., Bashir, S., Sharif, S., Ali, K., & Dogar, N.A. (2024). Synthesis of surfactant-assisted nickel ferrite nanoparticles (NFNPs@ surfactant) to amplify their application as an advanced electrode material for high-performance supercapacitors. *RSC Advances*, *14*(28), 20230-20239.

Naeem, M., Shah, N.A., Gul, I.H., & Maqsood, A. (2009). Structural, electrical and magnetic characterization of Ni–Mg spinel ferrites. *Journal of Alloys and Compounds*, *487*, 739-743. https://doi.org/10.1016/j.jallcom.2009.08.057.

Nassar, K.I., Teixeira, S.S., & Graça, M.P.F. (2025). Sol–gel-synthesized metal oxide nanostructures: advancements and prospects for spintronic applications-a comprehensive review. *Gels*, *11*(8), 657. https://doi.org/10.3390/gels11080657.

Noreen, Z., Ahmad, I., Siddiqui, F., Ziya, A.B., Abbas, T., & Bokhari, H. (2017). Size dependent structural, anti-bacterial and anti-biofilm properties of Er doped Li-Ni ferrites synthesized by the sol-gel auto-combustion route. *Ceramics International*, *43*(14), 10784-10790.

Oprica, L., Nadejde, C., Andries, M., Puscasu, E., Creanga, D., & Balasoiu, M. (2015). Magnetic contamination of environment--laboratory simulation of mixed iron oxides impact on microorganism cells. *Environmental Engineering & Management Journal*, *14*(3), 581-586.

Ortiz-Quiñonez, J.L., Pal, U., & Villanueva, M.S. (2018). Structural, magnetic, and catalytic evaluation of spinel Co, Ni, and Co–Ni ferrite nanoparticles fabricated by low-temperature solution combustion process. *ACS Omega*, *3*(11), 14986-15001.

Padmapriya, G., Manikandan, A., Krishnasamy, V., Jaganathan, S.K., & Antony, S.A. (2016). Spinel $Ni_xZn_{1-x}Fe_2O_4$ ($0.0 \leq x \leq 1.0$) nano-photocatalysts: synthesis, characterization and photocatalytic degradation of methylene blue dye. *Journal of Molecular Structure*, *1119*, 39-47. https://doi.org/10.1016/j.molstruc.2016.04.049.

Patil, M.R., Rendale, M.K., Mathad, S.N., & Pujar, R.B. (2017). FTIR spectra and elastic properties of Cd-substituted Ni–Zn ferrites. *International Journal of Self-Propagating High-Temperature Synthesis*, *26*(1), 33-39.

Peng, Y., Xia, C., Cui, M., Yao, Z., & Yi, X. (2021). Effect of reaction condition on microstructure and properties of (NiCuZn) Fe_2O_4 nanoparticles synthesized via co-precipitation with ultrasonic irradiation. *Ultrasonics Sonochemistry*, *71*, 105369. https://doi.org/10.1016/j.ultsonch.2020.105369.

Perez-Gonzalez, T., Jimenez-Lopez, C., Neal, A.L., Rull-Perez, F., Rodriguez-Navarro, A., Fernandez-Vivas, A., & Iañez-Pareja, E. (2010). Magnetite biomineralization induced by Shewanella oneidensis. *Geochimica et Cosmochimica Acta*, *74*(3), 967-979.

Phong, P.T., Nam, P.H., Phuc, N.X., Huy, B.T., Lu, L.T., Manh, D.H., & Lee, I.J. (2019). Effect of zinc concentration on the structural, optical, and magnetic properties of mixed Co-Zn ferrites nanoparticles synthesized by low-temperature hydrothermal method. *Metallurgical and Materials Transactions A*, *50*(3), 1571-1581.

Poongodi, R., Senguttuvan, S., & Sagayaraj, R. (2023). Exploring the decreasing coercivity properties of aluminum cobalt ferrites prepared by coprecipitation method. *Asian Journal of Chemistry*, *35*(6), 1525-1532.

Poongodi, R., Senguttuvan, S., Sebastian, S., & Sagayaraj, R. (2024). Analyzing the variations in electrical, structural and magnetic properties of zinc-doped MnFe2O4 ferrite obtained via co-precipitation. *Journal of the Australian Ceramic Society*, *60*(5), 1483-1494.

Prabhakaran, T., & Hemalatha, J. (2016). Combustion synthesis and characterization of cobalt ferrite nanoparticles. *Ceramics International*, *42*, 14113-14120.

Prajapati, N., Kumar, M., Pandey, V., Munjal, S., & Pandey, H. (2025). White LED-based photocatalytic treatment using recoverable cobalt ferrite nanoparticles. *Physica Scripta*, *100*(9), 095922.

Prakash, A., Jayarajan, D., Aravazhi, S., Chandrasekaran, G., & Nithya, R. (2022). Influence of Ce3+ substitution on magnetic properties and antibacterial activity of manganese ferrite nanoparticles synthesized by coprecipitation method. *Asian Journal of Chemistry*, *34*, 2288-2296.

Prakash, A., Sagayaraj, R., Jayarajan, D., Aravazhi, S., Sebastian, S., Sylvestre, S., & Nyanga, C. (2023). Influence of Ce3+ (rare earth element) on the structural, morphological, impedance, binding energy and ferrimagnetic properties of spinel ZnFe2O4 nanoparticles fabricated by the coprecipitation method: antibacterial activity. *Chemistry Africa*, *6*(3), 1269-1281.

Prasad, R.D., Karvekar, O.S., Pawar, P.B., Charmode, N., Shrivastav, O.P., Prasad, S.R., & Prasad, N.R. (2021). A review on nanotechnological aspects in veterinary medicine. *Research Journal of Life Sciences, Bioinformatics, Pharmaceuticals and Chemical Sciences*, *7*, 42-85.

Prasetya, N.P., Suharyana, S., Rikamukti, N., Riyatun, R., Utari, U., & Purnama, B. (2025). Synthesis temperature affects the crystalline and magnetic properties of strontium-modified cobalt ferrite nanoparticles. In *Materials Science Forum* (Vol. 1152, pp. 91-100). Trans Tech Publications Ltd.

Priya, A.S., Geetha, D., & Kavitha, N. (2019). Effect of Al substitution on the structural, electric and impedance behavior of cobalt ferrite. *Vacuum*, *160*, 453-460.

Rafienia, M., Bigham, A., & Hassanzadeh-Tabrizi, S.A. (2018). Solvothermal synthesis of magnetic spinel ferrites. *Journal of Medical Signals & Sensors*, *8*(2), 108-118.

Randhawa, B.S., & Gandotra, K. (2009). Synthesis of sodium ferrite by precursor and combustion methods: a comparative study. *Ceramics International*, *35*(1), 157-161.

Rathod, V., Anupama, A.V., Kumar, R.V., Jali, V.M., & Sahoo, B. (2017). Correlated vibrations of the tetrahedral and octahedral complexes and splitting of the absorption bands in FTIR spectra of Li-Zn ferrites. *Vibrational Spectroscopy*, *92*, 267-272.

Rawat, R.S. (2015). Dense plasma focus-from alternative fusion source to versatile high energy density plasma source for plasma nanotechnology. In *Journal of Physics: Conference Series* (Vol. 591, No. 1, p. 012021). IOP Publishing.

Rodríguez, A.A., Moreno-Trejo, M.B., Meléndez-Zaragoza, M.J., Collins-Martínez, V., López-Ortiz, A., Martínez-Guerra, E., & Sánchez-Domínguez, M. (2019). Spinel-type ferrite nanoparticles: synthesis by the oil-in-water microemulsion reaction method and photocatalytic water-splitting evaluation. *International Journal of Hydrogen Energy*, *44*(24), 12421-12429.

Roy, P., Hoque, S.M., Akter, S., Liba, S.I., & Choudhury, S. (2024). Study on the chemical co-precipitation synthesized CoFe2O4 nanoparticle for magnetocaloric performance in the vicinity of superparamagnetic blocking temperature. *Heliyon*, *10*(14), e34413. https://doi.org/10.1016/j.heliyon.2024.e34413.

Saeed, S., Sadiq, I., Hussain, S., Idrees, M., Sadiq, F., Riaz, S., & Naseem, S. (2020). La^{3+}-substituted β-ferrite: Investigation of structural, dielectric, FTIR and electrical polarization properties. *Journal of Alloys and Compounds*, *831*, 154854. https://doi.org/10.1016/j.jallcom.2020.154854.

Sagayaraj, R., Aravazhi, S., & Chandrasekaran, G. (2018). Synthesis, spectroscopy, and magnetic characterizations of PVP-assisted nanoscale particle. *Journal of Superconductivity and Novel Magnetism*, *31*, 3379-3386. https://doi.org/10.1007/s10948-018-4593-z.

Sagayaraj, R., Aravazhi, S., & Chandrasekaran, G. (2019a). Effect of zinc content on structural, functional, morphological, resonance, thermal and magnetic properties of Co1− xZnxFe2O4/PVP nanocomposites. *Journal of Inorganic and Organometallic Polymers and Materials*, *29*(6), 2252-2261. https://doi.org/10.1007/s10904-019-01183-3.

Sagayaraj, R., Aravazhi, S., Kumar, C.S., Kumar, S.S., & Chandrasekaran, G. (2019b). Tuning of ferrites (CoxFe3-xO4) nanoparticles by co-precipitation technique. *SN Applied Sciences*, *1*(3), 271. https://doi.org/10.1007/s42452-019-0244-7.

Sagayaraj, R., Aravazhi, S., Praveen, P., & Chandrasekaran, G. (2017). Structural, morphological and magnetic characters of PVP coated ZnFe2O4 nanoparticles. *Journal of Materials Science: Materials in Electronics*, *29*(3), 2151-2158.

Sagayaraj, R., Hilary, H.J.L., Xavier, S., Praveen, P., Elayakumar, K., &Yogambal, C. (2019c). Structural, vibrational, morphological and magnetic properties of copper ferrite nano particles ($Cu_{0.4M}Fe_{2.96M}O_4$) by co-precipitation method. *St. Joseph's Journal of Humanities and Science*, *6*(1), 58-62.

Sagayaraj, R., Jegadheeswari, M., Aravazhi, S., Chandrasekaran, G., & Dhanalakshmi, A. (2020). Structural, spectroscopic and magnetic study of nanocrystalline terbium-nickel ferrite by oxalate co-precipitation method. *Chemistry Africa*, *3*, 955-963.

Salavati-Niasari, M., Mahmoudi, T., Sabet, M., Hosseinpour-Mashkani, S.M., Soofivand, F., & Tavakoli, F. (2012). Synthesis and characterization of copper ferrite nanocrystals via coprecipitation. *Journal of Cluster Science*, *23*(4), 1003-1010.

Salavati-Niasari, M., Mir, N., & Davar, F. (2010). A novel precursor in preparation and characterization of nickel oxide nanoparticles via thermal decomposition approach. *Journal of Alloys and Compounds*, *493*(1-2), 163-168.

Salih, S.J., & Mahmood, W.M. (2023). Review on magnetic spinel ferrite (MFe_2O_4) nanoparticles: from synthesis to application. *Heliyon*, *9*(6), e16601. https://doi.org/10.1016/j.heliyon.2023.e16601.

Sangsuriyonk, K., Paradee, N., Rotjanasuworapong, K., &Sirivat, A. (2022). Synthesis and characterization of $Co_xFe_{1-x}Fe_2O_4$ nanoparticles by anionic, cationic, and non-ionic surfactant templates via co-precipitation. *Scientific Reports*, *12*(1), 4611.

Selvam, P.P., Rathinam, V., Ali Baig, A.B., & Sagayaraj, R. (2024). Enhanced structural, optical and magnetic properties of cobalt-doped zinc oxide nanoparticles synthesized via co-precipitation method. *Asian Journal of Chemistry*, *36,* 2160-2168.

Senthil, V.P., Gajendiran, J., Raj, S.G., Shanmugavel, T., Kumar, G.R., & Reddy, C.P. (2018). Study of structural and magnetic properties of cobalt ferrite ($CoFe_2O_4$) nanostructures. *Chemical Physics Letters*, *695*, 19-23. https://doi.org/10.1016/j.cplett.2018.01.057.

Sharma, R., Thakur, P., Kumar, M., Sharma, P., & Sharma, V. (2018). Nanomaterials for high frequency device and photocatalytic applications: Mg-Zn-Ni ferrites. *Journal of Alloys and Compounds*, *746*, 532-539. https://doi.org/10.1016/j.jallcom.2018.02.287.

Shukla, A., Bhardwaj, A.K., Singh, S.C., Uttam, K.N., Gautam, N., Himanshu, A.K., & Gopal, R. (2018). Microwave assisted scalable synthesis of titanium ferrite nanomaterials. *Journal of Applied Physics*, *123*(16), 161411. https://doi.org/10.1063/1.5008733.

Singh, T.A., Das, J., & Sil, P.C. (2020). Zinc oxide nanoparticles: a comprehensive review on its synthesis, anticancer and drug delivery applications as well as health risks. *Advances in Colloid and Interface Science*, *286*, 102317. https://doi.org/10.1016/j.cis.2020.102317.

Sinthiya, M.M.A., Ramamurthi, K., Mathuri, S., Manimozhi, T., Kumaresan, N., Margoni, M.M., & Karthika, P.C. (2015). Synthesis of zinc ferrite ($ZnFe_2O_4$) nanoparticles with different capping agents. *International Journal of ChemTech Research*, *7*, 2144-2149.

Sivakumar, P., Ramesh, R., Ramanand, A., Ponnusamy, S., &Muthamizhchelvan, C. (2011). Synthesis and characterization of nickel ferrite magnetic nanoparticles. *Materials Research Bulletin*, *46*(12), 2208-2211.

Somvanshi, S.B., Khedkar, M.V., Kharat, P.B., & Jadhav, K.M. (2020). Influential diamagnetic magnesium (Mg^{2+}) ion substitution in nano-spinel zinc ferrite ($ZnFe_2O_4$): thermal, structural, spectral, optical and physisorption analysis. *Ceramics International*, *46*(7), 8640-8650.

Soufi, A., Hajjaoui, H., Elmoubarki, R., Abdennouri, M., Qourzal, S., & Barka, N. (2021). Spinel ferrites nanoparticles: Synthesis methods and application in heterogeneous Fenton oxidation of organic pollutants–A review. *Applied Surface Science Advances*, *6*, 100145. https://doi.org/10.1016/j.apsadv.2021.100145.

Srinivas, C., Deepty, M., Kumar, E.R., Prasad, S.A.V., Tirupanyam, B.V., Meena, S.S., Prajapat, C.L., & Sastry, D.L. (2019). Rietveld refinement and FTIR spectroscopic studies of Ni2+-substituted Zn-ferrite nanoparticles. *Applied Physics A*, *125*(8), 554. https://doi.org/10.1007/s00339-019-2840-1.

Su, M., He, C., Sharma, V.K., Abou Asi, M., Xia, D., Li, X.Z., Deng, H., & Xiong, Y. (2012). Mesoporous zinc ferrite: synthesis, characterization, and photocatalytic activity with H2O2/visible light. *Journal of Hazardous Materials*, *211*, 95-103.

Sundararajan, M., Kennedy, L.J., Nithya, P., Vijaya, J.J., &Bououdina, M. (2017). Visible light driven photocatalytic degradation of rhodamine B using Mg doped cobalt ferrite spinel nanoparticles synthesized by microwave combustion method. *Journal of Physics and Chemistry of Solids*, *108*, 61-75. https://doi.org/10.1016/j.jpcs.2017.04.002.

Sutka, A., Mezinskis, G., Zamovskis, M., Jakovlevs, D., & Pavlovska, I. (2013). Monophasic $ZnFe_2O_4$ synthesis from a xerogel layer by auto combustion. *Ceramics International*, *39*(7), 8499-8502.

Thakur, P., Chahar, D., Taneja, S., Bhalla, N., & Thakur, A. (2020). A review on MnZn ferrites: synthesis, characterization and applications. *Ceramics International*, *46*(10), 15740-15763.

Tiwari, R., De, M., Tewari, H.S., & Ghoshal, S.K. (2020). Structural and magnetic properties of tailored NiFe2O4 nanostructures synthesized using auto-combustion method. *Results in Physics*, *16*, 102916. https://doi.org/10.1016/j.rinp.2019.102916.

Torruella, P., Ruiz-Caridad, A., Walls, M., Roca, A.G., López-Ortega, A., Blanco-Portals, J., López-Conesa, L., Nogués, J., Peiró, F., & Estrade, S. (2018). Atomic-scale determination of cation inversion in spinel-based oxide nanoparticles. *Nano Letters*, *18*(9), 5854-5861.

Veeramani, T., Venkataraju, C., Porkalal, V., & Sagayaraj, R. (2023). Effect of ZnO on the structural and magnetodielectric properties of MgFe2O4 nanocomposite prepared by sol-gel method. *Asian Journal of Chemistry*, *35*(9), 2069-2077.

Venkatesh, N., Kumar, D.R., Goud, S., Ahmad, S.I., Veerasomaiah, P., & Ravinder, D. (2023). Structural, photocatalytic, electromagnetic properties of rare-earth metal Gd-doped Mg nanoferrites synthesized by citrate gel auto-combustion method. *Chemical Papers*, *77*(5), 2749-2767.

Venkatesh, N., Kumar, N.H., Goud, S., Ravinder, D., Somaiah, P.V., Babu, T.A., & Prasad, N.V.K. (2021). FTIR, optical, electrical and magnetic properties of SM3+ doped MG nano ferrites. *Biointerface Research in Applied Chemistry*, *11*(6), 15037-15050.

Vidya, S.T., Subba, R.T., & Raghuram, N. (2020). Temperature dependent structural, morphological, FTIR, optical, magnetic properties of NiMgZn ferrites. *Наносистемы: физика, химия, математика*,*11*(4), 434-443. https://doi.org/10.17586/2220-8054-2020-11-4-434-443.

Vinosha, P.A., & Das, S.J. (2018). Investigation on the role of pH for the structural, optical and magnetic properties of cobalt ferrite nanoparticles and its effect on the photo-fenton activity. *Materials Today: Proceedings*, *5*(2), 8662-8671.

Vishwas, M., Babu, K.V., Gowda, K.A., & Gandla, S.B. (2022). Synthesis, characterization and photo-catalytic activity of magnetic CoFe2O4 nanoparticles prepared by temperature-controlled co-precipitation method. *Materials Today: Proceedings*, *68*, 497-501. https://doi.org/10.1016/j.matpr.2022.07.429.

Wu, R., Qu, J., He, H., & Yu, Y. (2004). Removal of azo-dye Acid Red B (ARB) by adsorption and catalytic combustion using magnetic CuFe2O4 powder. *Applied Catalysis B: Environmental*, *48*(1), 49-56.

Xavier, S., Thankachan, S., Jacob, B.P., & EM, M. (2013). Effect of sintering temperature on the structural and magnetic properties of cobalt ferrite nanoparticles. *Nanosystems: Physics, Chemistry, Mathematics*, *4*(3), 430-437.

Xu, J., Yang, H., Fu, W., Du, K., Sui, Y., Chen, J., Zeng, Y., Li, M., & Zou, G. (2007). Preparation and magnetic properties of magnetite nanoparticles by sol–gel method. *Journal of Magnetism and magnetic Materials*, *309*(2), 307-311.

Yadav, N.G., Chaudhary, L.S., Sakhare, P.A., Dongale, T.D., Patil, P.S., & Sheikh, A.D. (2018a). Impact of collected sunlight on ZnFe2O4 nanoparticles for photocatalytic application. *Journal of Colloid and Interface Science*, *527*, 289-297.

Yadav, R.S., Kuřitka, I., Vilcakova, J., Havlica, J., Kalina, L., Urbánek, P., Machovský, M., Skoda, D., Masar, M., & Holek, M. (2018b). Sonochemical synthesis of Gd3+ doped CoFe2O4 spinel ferrite nanoparticles and its physical properties. *Ultrasonics Sonochemistry*, *40*, 773-783. https://doi.org/10.1016/j.ultsonch.2017.08.024.

Zheng, L., Fang, K., Zhang, M., Nan, Z., Zhao, L., Zhou, D., Zhu, M., & Li, W. (2018). Tuning of spinel magnesium ferrite nanoparticles with enhanced magnetic properties. *RSC Advances*, *8*, 39177-39181.

Zhou, W., He, W., Zhang, X., Yan, S., Sun, X., Tian, X., & Han, X. (2009a). Biosynthesis of iron phosphate nanopowders. *Powder Technology*, *194*(1-2), 106-108.

Zhou, W., He, W., Zhong, S., Wang, Y., Zhao, H., Li, Z., & Yan, S. (2009b). Biosynthesis and magnetic properties of mesoporous Fe_3O_4 composites. *Journal of Magnetism and Magnetic Materials*, *321*(8), 1025-1028.